Coherent bremsstrahlung, coherent pair production, birefringence, and polarimetry in the 20-170 GeV energy range using aligned crystals

Apyan, A.; Ketel, T.J.; van Rens, B.

published in
Physical Review Special Topics. Accelerators and Beams
2008

DOI (link to publisher)
10.1103/PhysRevSTAB.11.041001

document version
Publisher's PDF, also known as Version of record

Coherent bremsstrahlung, coherent pair production, birefringence, and polarimetry in the 20–170 GeV energy range using aligned crystals

A. Apyan,[1,*] R. O. Avakian,[1] B. Badelek,[2] S. Ballestrero,[3,¶] C. Biino,[4,5] I. Birol,[6] P. Cenci,[7] S. H. Connell,[8] S. Eichblatt,[6] T. Fonseca,[6] A. Freund,[9] B. Gorini,[5] R. Groess,[10] K. Ispirian,[1] T. J. Ketel,[11] Yu. V. Kononets,[12] A. Lopez,[13] A. Mangiarotti,[14] B. van Rens,[11] J. P. F. Sellschop,[10,†] M. Shieh,[6] P. Sona,[14] V. Strakhovenko,[15] E. Uggerhøj,[16,‡] U. I. Uggerhøj,[17] G. Unel,[18] M. Velasco,[5,§] Z. Z. Vilakazi,[10,‖] and O. Wessely[2]

(NA59 Collaboration)

[1]*Yerevan Physics Institute, Yerevan, Armenia*
[2]*Uppsala University, Uppsala, Sweden*
[3]*INFN and University of Firenze, Firenze, Italy, and CERN, Geneva, Switzerland*
[4]*INFN and University of Torino, Torino, Italy*
[5]*CERN, Geneva, Switzerland*
[6]*Northwestern University, Evanston, Illinois 60208, USA*
[7]*INFN, Perugia, Italy*
[8]*School of Physics, University of the Witwatersrand, Johannesburg, South Africa*
[9]*ESRF, Grenoble, France*
[10]*Schonland Research Centre, University of the Witwatersrand, Johannesburg, South Africa*
[11]*NIKHEF, Amsterdam, The Netherlands*
[12]*Kurchatov Institute, Moscow, Russia*
[13]*University of Santiago de Compostela, Santiago de Compostela, Spain*
[14]*INFN and University of Firenze, Firenze, Italy*
[15]*Institute of Nuclear Physics, Novosibirsk, Russia*
[16]*Institute for Storage Ring Facilities, University of Aarhus, Denmark*
[17]*University of Aarhus, Aarhus, Denmark*
[18]*University of California at Irvine, Physics Department, Irvine, California 92697, USA*

(Received 2 March 2008; published 16 April 2008)

The processes of coherent bremsstrahlung (CB) and coherent pair production (CPP) based on aligned crystal targets have been studied in the energy range 20–170 GeV. The experimental arrangement allowed for measurements of single photon properties of these phenomena including their polarization dependences. This is significant as the theoretical description of CB and CPP is an area of active debate and development. With the approach used in this paper, both the measured cross sections and polarization observables are predicted very well. This indicates a proper understanding of CB and CPP up to energies of 170 GeV. Birefringence in CPP on aligned crystals is applied to determine the polarization parameters in our measurements. New technologies for high-energy photon beam optics including phase plates and polarimeters for linear and circular polarization are demonstrated in this experiment. Coherent bremsstrahlung for the strings-on-strings (SOS) orientation yields a larger enhancement for hard photons than CB for the channeling orientations of the crystal. Our measurements and our calculations indicate low photon polarizations for the high-energy SOS photons.

DOI: 10.1103/PhysRevSTAB.11.041001 PACS numbers: 78.70.−g, 61.85.+p, 78.20.Fm, 95.75.Hi

I. INTRODUCTION

The demand for high-energy circularly polarized photon beams has increased with the need to study gluon related features of the nucleon. The so-called "spin crisis of the nucleon" and its connection to the gluon polarization has attracted much attention [1]; for example, experiments to determine the gluon spin density of the nucleon [1–3] from polarized virtual photon-gluon fusion, and polarized virtual photoproduction of high transverse momentum mesons [4]. Future experiments will require intense high-energy photon beams with a high degree of circular polar-

[*] Now at Northwestern University, Evanston, IL, USA.
[†] Deceased.
[‡] Co-spokesperson.
[§] Co-spokesperson.
Now at Northwestern University, Evanston, IL, USA.
[‖] Now at University of Cape Town, Cape Town, South Africa.
[¶] Now at University of the Witwatersrand, Johannesburg, South Africa.

ization. A well-known method to produce circularly polarized photons is the interaction of longitudinally polarized electrons with crystalline media, where the emitted photons are circularly polarized due to conservation of angular momentum [5]. Specifically, theoretical calculations [6,7] predict that coherent bremsstrahlung (CB) and channeling radiation in crystals by longitudinally polarized electrons are also circularly polarized, and this can be used to enhance the number of high-energy circularly polarized photons. The subject of interactions of relativistic particles with strong crystalline fields has been recently reviewed [8]. Currently, the highest energy polarized electron beam available is 45 GeV [9,10]. Photons that will allow $\gamma g \rightarrow c\bar{c}$ in $\Lambda_c D$ production with a four-momentum fraction of the gluon of η have a threshold energy of $9.2/\eta$ GeV. Therefore, the available polarized electron beams cannot produce polarized photons that are sufficiently energetic, that is above 92 GeV, to investigate the gluon spin contribution to the proton by the above-mentioned reaction for η values of about 0.1.

Unpolarized electron beams are available to much higher energies, for example, energies of up to 250 GeV at CERN and 125 GeV at FNAL. Linearly polarized photons may be produced from such beams by CB. It is therefore of interest to investigate the possible conversion of this linear polarization to circular, and to develop polarimetry techniques at these very high photon energies. CB radiation differs from incoherent bremsstrahlung (ICB) in an amorphous target in that the cross section is substantially enhanced with relatively sharp peaks in the photon spectrum. The position of these peaks can be tuned by adjusting the electron beam incidence angle with respect to the major planes of the lattice. New features of coherent high-energy photon emission develop at higher electron energies. For certain geometries for the incident electron beam with respect to the aligned crystal target, the so-called ''strong field'' effects become important. A special case is found if the electron beam is incident very close to the plane (within the planar channeling critical angle) and also closely aligned to a major axis (but beyond the axial channeling critical angle). Here the electrons interact dominantly with successive atomic strings in the plane. This orientation was aptly described by the term ''string-of-strings'' (SOS) by Lindhard, a pioneer of beam-crystal phenomena [11]. The polarization features of this SOS radiation require further investigation. In conclusion, a study of the above-mentioned phenomena constitutes an opportunity to benchmark the latest theoretical approaches that describe CB and also the related process of coherent pair production (CPP) at these energies.

Accordingly, this paper has three distinct sections. The first section studies birefringent effects in CPP by photons in the 20–170 GeV energy range incident on aligned crystals. As a by-product, a new crystal polarimetry technique is established. The second section extends the investigation of birefringence by aligned crystals and demonstrates the conversion of linear polarization to circular polarization for the CB photons. The crystal polarimetry technique is here extended to quantify also circular polarization. The third section addresses the issue of the polarization of SOS radiation. Also in this section it is demonstrated that the theory which is discussed accurately describes the observations. The theoretical calculations cover the cross sections for CB and SOS radiation for the photon generation, the cross section for CPP for the polarimetry, and the linear to circular polarization conversion. Simulations based on the theoretical calculations therefore predict the measured polarization observables. The good agreement between our measurements and the simulations indicate that, even for the strong field case, the theoretical description is reliable.

This work focuses both on cross sections and polarization phenomena in CB and CPP at high energies in oriented single crystals. The CB and CPP theories are constructed in the framework of the first Born approximation in the crystal potential. These theories are well established and were experimentally investigated for up to a few tens of GeV electrons and photons. The theoretical description of those phenomena in oriented single crystals becomes more complicated at higher energies. The processes have strong angular and energy dependence and the validity conditions of the Born approximation no longer hold at very high energies and small incidence angles with respect to the crystal axes and planes. The onset of this problem for the description of radiation emission and pair production (PP) has the characteristic angle $\theta_v = U_0/m$ [12], where U_0 is the plane potential well depth, m is the electron rest mass, and $\hbar = c = 1$. The radiation and pair-production processes can be described by the CB and CPP theory for the incidence angles with respect to the crystal axes/planes $\theta \gg \theta_v$. For angles $\theta \sim \theta_v$ and $\theta < \theta_v$ a different approach, known as the quasiclassical description, is used. In this approach the general theory of radiation and pair production is developed based on the quasiclassical operator method [12].

II. PRODUCTION OF HIGH-ENERGY PHOTON BEAMS

As described below, the so-called point effect (PE) orientation of the crystal was used in the first section of the experiment, where linear polarization studies of high-energy CB photons were performed and birefringent effects in pair production on aligned crystals were studied. This section of the experiment also leads to a new polarimetry technique [13].

The same orientation was also used in the second section of the experiment, where the conversion of the linear polarization to circular polarization induced by a birefringent effect in an aligned single crystal was studied [14].

For the third section of the experiment, the crystal orientation appropriate for SOS radiation was used [15]. This radiation production scenario is also treated below.

A. Linearly polarized CB photons

In the production of photon beams, single crystals can play an important role by exploiting coherent and strong field effects that arise for oriented incidence in the interaction of radiation and matter in crystalline materials [16]. The CB method is a well established technique for obtaining linearly polarized photons starting from unpolarized electrons [17–20]. An electron impinging on a crystal will interact coherently with the electric fields of the atoms in aligned crystal planes. If the Laue condition is satisfied, the bremsstrahlung photons will be emitted at specific energies corresponding to the selected vectors of the reciprocal lattice. In the so-called PE orientation of the crystal, the direction of the electron beam has a small angle with respect to a chosen crystallographic plane and a relatively large angle with the crystallographic axes that are in that plane. For this PE orientation of the single crystal, only one reciprocal lattice vector contributes to the CB cross section. The CB radiation from a crystal aligned in this configuration is more intense than the ICB radiation in amorphous media and a high degree of linear polarization can be achieved [18]. The maximum polarization and the maximum peak intensity occur at the same photon energy, and this energy can be selected by choosing the orientation of the lattice planes with respect to the incoming electron beam. This property has been used previously to achieve photon beams with up to 70% linear polarization starting from 6 GeV electrons [21], and up to 60% linear polarization starting from 80 GeV electrons [22].

The emission mechanism of the high-energy photons (CB) is connected to the periodic structure of the crystal [18]. The peak energy of the CB photons, E_γ, is determined from the condition (the system of units used here has $\hbar = c = 1$)

$$\frac{1}{|q_\parallel|} = 2\lambda_c \gamma \frac{E_0 - E_\gamma}{E_\gamma}, \tag{1}$$

where $|q_\parallel|$ is the component of the recoil momentum of the nucleus parallel to the initial electron velocity and the other symbols have their usual meanings. Recall, in a crystal possible values of $\mathbf{q}$, from which the contribution to the coherent radiation comes, are discrete: $\mathbf{q} = \mathbf{g}$ [18], where $\mathbf{g}$ is a reciprocal lattice vector of the crystal. The minimal reciprocal lattice vector giving rise to the main CB peak is given by

$$|g_\parallel|_{\min} = \frac{2\pi}{d}\Theta. \tag{2}$$

For the PE orientation, d is the interplanar distance and $\Theta = \psi$, the electron incident angle with respect to the plane.

The position of the hard photon peak can be selected by simultaneous solution of the last two equations:

$$\Theta = \frac{d}{4\pi\gamma\lambda_c}\frac{E_\gamma}{E_0 - E_\gamma}. \tag{3}$$

The coherence length determines the effective longitudinal dimension of the interaction region for the phase coherence of the radiation process:

$$l_{\text{coh}} = \frac{1}{|q_\parallel|}. \tag{4}$$

The relative merits of different single crystals as CB radiators have been investigated in the past [23]. The silicon crystal stands out as a good choice due to its availability, ease of growth, and low mosaic spread (high lattice quality). A Si crystal thickness of 1.5 cm was selected to achieve a relatively low photon multiplicity and reasonable photon emission rate. This multiplicity is shown in Fig. 1 to reside dominantly in lower energy photons.

The multiplicity is the weighted average of the number of photons per incident electron:

$$M = \frac{\sum_{i=1}^{n} iN_i}{\sum_{i=1}^{n} N_i}, \tag{5}$$

where $i = 1, 2, 3, \ldots, n$ is the number of radiated photons (with an energy above the E_γ threshold) per electron and N_i is the number of electrons radiating the number of photons, i. For example, N_1 is the number of electrons radiating only one photon, N_2 is the number of electrons radiating two photons, etc. $N = \sum_i N_i$ is the total number of primary electrons.

For a 178 GeV electron beam making an angle of 5 mrad from the ⟨001⟩ crystallographic axis and about 70 μrad from the (110) plane, the resulting photon beam polarization spectrum was predicted to yield maximum polarization of about 55% in the vicinity of 70 GeV, as seen in Fig. 2.

For this choice of crystal orientation, the incidence angles of electrons and photons to the crystal plane become

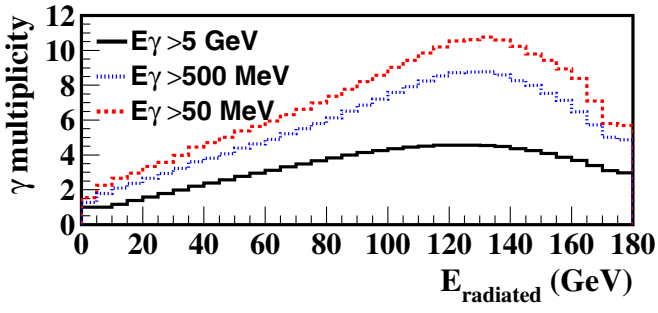

FIG. 1. (Color) Monte Carlo prediction for photon multiplicity vs total radiated energy using different photon energy cutoff values.

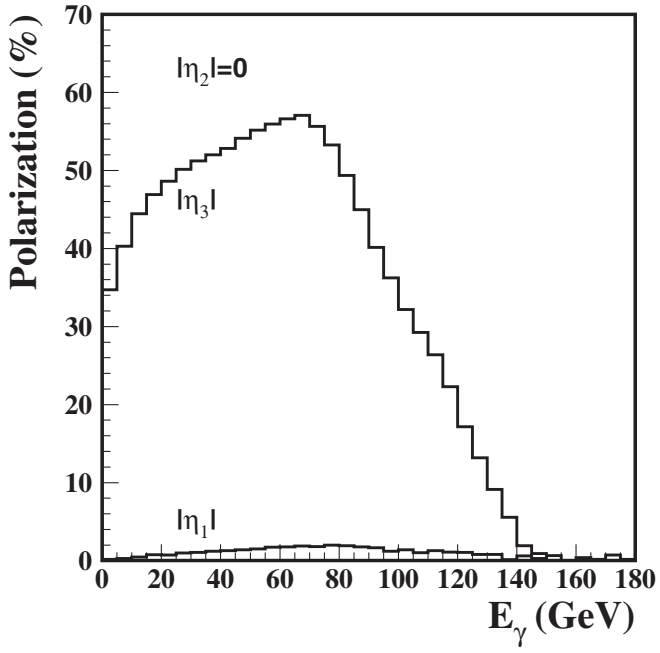

FIG. 2. Theoretical calculation of the polarization for 178 GeV photon beam for the radiator conditions mentioned in the text.

comparable with the radiation and pair-production characteristic angle θ_v. In case of the (110) plane of the silicon crystal, we find $\theta_v = 42$ μrad. In fact, part of the incident electron beam penetrates the crystal with angles both less and greater than θ_v, because of the angular divergence of the electron beam.

In the simulations presented here, a Monte Carlo approach was used to model the divergence of the electron and photon beams, and the relevant theories (CB and CPP or the quasiclassical theory) are selected as appropriate for accurate and fast calculation. The details may be found in Ref. [24] and references therein. Briefly, the random trajectory method is deployed, where each particle is described by its history in propagation through the aligned crystals. Each particle history i is represented by the array $\mathbf{S}_j^i$ denoting the state of particle before j_{th} interaction [25]:

$$\mathbf{S}_j^i = (\mathbf{r}_j^i, \boldsymbol{\Omega}_j^i, \boldsymbol{\eta}_j^i, E_j^i, q_j^i), \tag{6}$$

where $\mathbf{r}_j^i$, $\boldsymbol{\Omega}_j^i$, $\boldsymbol{\eta}_j^i$, E_j^i, and q_j^i represent the electron or photon position, direction, polarization, energy, and charge before each interaction acts, respectively. The simulation code calculates the new state of particles after each interaction acts. A history is terminated when the particle energy drops below a low energy cutoff, or when the particle moves outside the target. All successive interactions of electrons and photons with atoms are simulated, such as coherent and incoherent bremsstrahlung and pair production. The Monte Carlo code tracks all of the charged particles and photons generated through the aligned crystal by taking into account the parameters of the incoming beam, multiple scattering, energy loss, emission angles, transverse dimension of the propagating beams, and the linear polarization of the photons produced. The corresponding energy losses, polarization, and scattering angles are determined from the appropriate differential cross sections of CB and CPP. It will be shown later that this approach has lead to a very good agreement between the theoretical predictions and the data.

B. Enhanced production of SOS photons

The character of the radiation, including its linear polarization, is changed when the direction of the electron (i) has a small angle with a crystallographic axis and (ii) is parallel with the plane that is formed by the atomic strings along the chosen axes. This is the so-called SOS orientation. It produces a harder photon spectrum than the CB case because the coherent radiation arises from successive scattering off the axial potential, which is deeper than the planar potential. The radiation phenomena in single crystals aligned in the SOS mode have been under active theoretical investigation since the discovery of two distinct photon peaks, one in the low energy region and one in the high-energy region of the radiated energy spectrum for about 150 GeV electrons traversing a diamond crystal [26]. It was established that the hard photon peak was a single photon peak [16]. However, the radiated photons were generally emitted with significant multiplicity in such a way that a hard photon would be accompanied by a few low energy photons. It will be seen later that two different mechanisms are responsible for the soft and the hard photons. In the former case, it is planar channeling (PC) radiation, while in the latter case, it is SOS radiation. An additional intriguing feature of SOS radiation at these energies ($E_\gamma \approx 120$ GeV) is that it occurs at the onset of a regime where strong field effects need to be taken into account. These fields are characterized by the parameter $\chi = \gamma\mathcal{E}/\mathcal{E}_0$, where $\gamma\mathcal{E}$ is the boosted crystal field in the electron frame and $\mathcal{E}_0$ is the Schwinger field. This is defined as the field which separates a virtual pair by the electron Compton wavelength, $\mathcal{E}_0 = m/e\lambda_c$ [27–29]. The quantum suppression of radiation expected under these conditions [12,30,31] was evidenced [8,16,32], as well as other effects [33,34]. Other situations where such conditions have been achieved are terawatt laser fields and above barrier very heavy ion collisions.

The issue of the polarization of SOS radiation also came into question. Early experiments with electron beams of up to 10 GeV in single crystals showed a smaller linear polarization of the more intense radiation in the SOS orientation than in the PE orientation (see [35] and references therein). The first measurements of linear polarization for high-energy photons ($E_\gamma \approx 50$–150 GeV) were consistent with a high degree of linear polarization of the radiated photons [36]. At this stage the theoretical prediction of the SOS hard photon polarization was unresolved. It

was however clear that the photons emitted by the PC mechanism would be linearly polarized. The polarimeter in this experiment recorded the integral polarization for a given radiated energy, which was likely to have a multiphoton character. This experiment therefore could not be considered conclusive as it did not separate the PC and SOS components and the extent to which pileup from the low energy photons perturbed the high-energy part of the total radiated energy spectrum was not resolved. These results therefore required more theoretical and experimental investigation.

A theory of photon emission by electrons along the SOS orientation of single crystals has since been developed. The theory takes into account the change of the effective electron mass in the fields due to the crystallographic planes and the crossing of the atomic strings [37]. Those authors show that the SOS specific potential affects the high-energy photon emission and also gives an additional contribution in the low energy region of the spectrum. In Refs. [38,39], the linear polarization of the emitted photons was derived and analyzed for different beam energies and crystal orientations. The predicted linear polarization of hard photons produced using the SOS orientation of the crystal is small compared to the comparable case using the PE orientation of the crystal. On the other hand, the additional soft photons produced with SOS orientation of the crystal are predicted to exhibit a high degree of polarization.

The peak energy of the SOS photons, E_γ, is determined from the same condition as for CP photons [Eq. (1)]. However, for the SOS orientation, d is the spacing between the axes (strings) forming the planes, and $\Theta = \theta$, the electron incident angle with respect to the axis.

With the appropriate choice of θ the intensity of the SOS radiation may exceed the Bethe-Heitler radiation [incoherent bremsstrahlung (ICB)] by an order of magnitude.

When a thin silicon crystal is used with an electron beam of energy $E_0 = 178$ GeV incident along the SOS orientation, within the (110) plane and with an angle of $\theta = 0.3$ mrad to the $\langle 100 \rangle$ axis, the hard photon peak position is expected at $E_\gamma = 129$ GeV.

In the current experiment, a 1.5 cm thick silicon crystal was used in the SOS orientation as mentioned above. Under this condition the radiation is expected to be enhanced by about a factor 20 with respect to the ICB for a randomly oriented crystalline Si target of the same thickness.

The radiation spectrum with the crystal aligned in SOS orientation has in addition to the CB radiation a strong component at a low energy which is characteristic of planar channeling (PC) radiation. As the electron direction lines up with a crystallographic plane in the SOS orientation, the planar channeling condition is fulfilled. For channeling radiation, the coherence length is much longer than the interatomic distances and the long range motion, characteristic of planar channeled electrons, becomes dominant over short range variations with the emission of low energy photons. Theoretical calculations [40,41] predict a more intense soft photon contribution (PC) with a high degree of linear polarization of up to 70%.

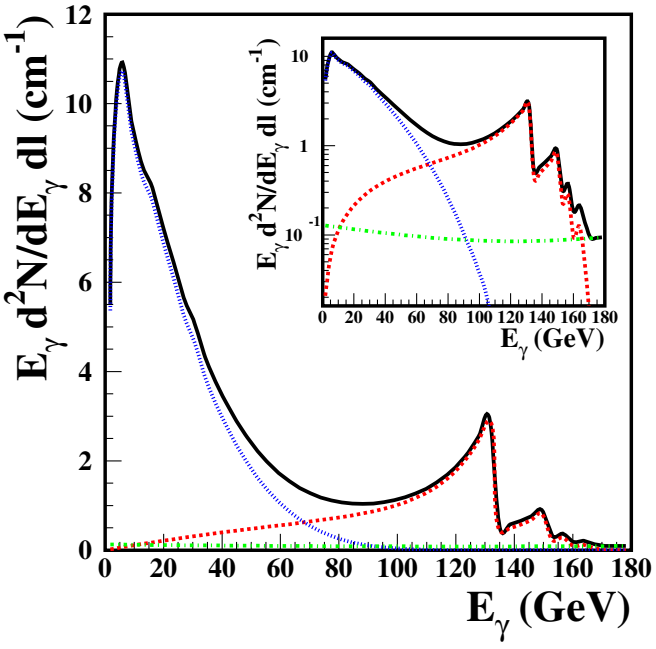

FIG. 3. (Color) Photon power yield, $E_\gamma d^2N/dE_\gamma dl$, per unit of thickness for a thin silicon crystal in the SOS orientation. The solid curve represents the total of the contributions from ICB (green dash-dotted), PC (blue dotted), and SOS (red dashed) radiation. The inset is a logarithmic representation and shows the flat incoherent contribution and the enhancement with a factor of about 20 for SOS radiation at 129 GeV.

The calculations of the enhancements of both the low energy and the high-energy components of the radiation emission for the SOS orientation under conditions applicable to this experiment are presented in Fig. 3. Where $E_0 = 178$ GeV electron beam incidences the (110) plane and at an angle of $\theta = 0.3$ mrad to the $\langle 100 \rangle$ axis. At low energy the PC radiation dominates and at high energies the SOS radiation peaks.

III. BEAM-OPTIC ELEMENTS FOR VERY HIGH-ENERGY PHOTON BEAMS

In this work the polarization observables for high-energy photons produced either by CB or SOS radiation are determined using the birefringence phenomena in CPP on aligned crystals. The study of the conversion of linear to circular polarization is based on the same birefringent effect in CPP. The experiments and their theoretical simulation therefore represent simultaneously a test of the theoretical understanding as well as development of new beam-optic elements based on crystal techniques.

A. Birefringence in CPP and crystal polarimetry

Historically, the pair conversion in single crystals was proposed, and later successfully used in the 1960s as a method to measure linear polarization for photons in the 1–6 GeV range [42]. It was predicted theoretically and later verified experimentally [43] that the pair-production cross section and the sensitivity to photon polarization increases with increasing energy. Therefore, at sufficiently high photon energies, a new polarization technique based on this effect can be constructed, which will become competitive to other techniques, such as pair production in amorphous media and photonuclear methods.

In the first part of the experiment, the cross section for CPP by polarized photons incident on the aligned "analyzer" crystals (germanium and diamond) was measured, for different carefully selected crystallographic orientations. This process can be effectively viewed as the imaginary part of the refractive index, as it leads to an attenuation of the photon beam. It constitutes a birefringence phenomenon, as the imaginary part of the refractive index will differ as a function of the angle between the plane of polarization of the photon beam and a specific crystallographic orientation of the analyzer crystal. A polarimeter was constructed by measuring the energy dependent asymmetry with respect to the two most distinct orientations of the analyzer crystal for pair production.

The theoretical comparison to the data could validate the calculation of the energy dependence of the cross section and the polarization of photons produced by coherent bremsstrahlung as well as the calculation of coherent pair production for polarized photons incident on crystals of different crystallographic orientations.

The photon polarization is expressed using the Stoke's parametrization with the Landau convention, where the total elliptical polarization is decomposed into two independent linear components and a circular component. Referred to our geometry the parameter η_1 describes the linear polarization of the beam polarized in the direction of 45° to the reaction plane of the radiator, while the parameter η_3 describes the linear polarization in the direction parallel or perpendicular to the reaction plane of the radiator. The parameter η_2 describes the circular polarization. The total polarization is then written

$$P_{\text{linear}} = \sqrt{\eta_1^2 + \eta_3^2}, \qquad P_{\text{circular}} = \sqrt{\eta_2^2}, \qquad P_{\text{total}} = \sqrt{P_{\text{linear}}^2 + P_{\text{circular}}^2}. \tag{7}$$

The radiator angular settings were chosen to have the total linear polarization from CB radiation purely along η_3. Two distinct measurements were made, one to show that the η_1 component of the polarization was consistent with zero and another to find the expected η_3 component of polarization as shown in Fig. 2. The Monte Carlo calculations used to obtain this prediction took into account the divergence of the electron beam (48 μrad horizontally and 33 μrad vertically) and the 1% uncertainty in its 178 GeV energy. To optimize the processing time of the Monte Carlo simulation, minimum energy cuts of 5 GeV for the electrons and 500 MeV for the photons were applied. We were, therefore, able to predict both the total radiated energy spectrum and the energy spectrum of individual photons.

The polarization dependence of the pair-production cross section and the birefringent properties of crystals are key elements of the photon polarization measurement. The imaginary parts of the refraction indices are related to the pair-production cross section. This cross section is sensitive to the relative angle between a crystal plane of a specific symmetry and the plane of linear polarization of the incident photon. In essence, the two orthogonal directions where these two planes are either parallel or perpendicular to each other yield the greatest difference in pair-production cross section.

Thus, the dependence of the CPP cross section on the linear polarization of the photon beam makes an oriented single crystal suitable as an efficient polarimeter for high-energy photons. The existence of a strong anisotropy for the production of the e^+e^- pairs during their formation is the reason for the polarization dependent CPP cross section of photons passing through oriented crystals. This means that perfect alignment along a crystallographic axis is not an efficient analyzer orientation due to the approximate cylindrical symmetry of the crystal around atomic strings. However, for small angles of the photon beam with respect to the crystallographic symmetry directions, the conditions for the formation of the e^+e^- pairs prove to be very anisotropic. As it turns out, the orientations with the highest analyzing power are those where the e^+e^- pair formation zone is not only highly anisotropic but also inhomogeneous with maximal fluctuations of the crystal potential along the electron path. At the crystallographic axes, the potential is largest and so are the fluctuations. These conditions are related to the ones of the SOS orientation: (i) a small angle to a crystallographic axis to enhance the pair-production process by the large fluctuations and (ii) a smaller angle to the crystallographic plane to have a long but still anisotropic formation zone for CPP.

We therefore studied the pairs created in a second aligned crystal, called the *analyzer* crystal. In this study, the experimentally relevant quantity is the asymmetry, A, between the pair-production cross sections, σ, of parallel and perpendicular polarized photons, where the polarization direction is measured with respect to the $\langle 110 \rangle$ crystallographic plane of the analyzer crystal. This asymmetry is related to the linear photon polarization, P_1, through the equation

$$A \equiv \frac{\sigma(\gamma_\perp \to e^+e^-) - \sigma(\gamma_\parallel \to e^+e^-)}{\sigma(\gamma_\perp \to e^+e^-) + \sigma(\gamma_\parallel \to e^+e^-)} = R \times P_1. \tag{8}$$

Here R is the so-called "analyzing power" of the second crystal. The analyzing power is in fact the asymmetry expected for a 100% linearly polarized photon beam. It will be seen that, for the conditions of this experiment, and using the theory described, this quantity can be reliably computed using Monte Carlo simulations. In this polarimetry method, the crystal with the highest possible analyzing power is preferred in order to achieve a fast determination of the photon polarization.

If one defines a parameter to measure the pair energy asymmetry as the ratio of the energy of one of the pairs, E^-, to the energy of the incoming photon, E_γ, as

$$y \equiv E^-/E_\gamma, \tag{9}$$

then one may calculate the dependence of the pair-production rate on this ratio, y, as shown in Fig. 4 (zero asymmetry corresponds to $y = \frac{1}{2}$).

By comparing the rates for the photon polarization parallel (solid line) and perpendicular (dashed line) to the crystallographic plane, we observe that the largest difference arises for $0.4 \leq y \leq 0.6$. Therefore the pair-production asymmetry may be maximized by selecting the subset of events where the e^+e^- pairs have similar energies. This method of choosing the pairs to enhance the analyzing power is called the "quasisymmetrical pair selection method" [44]. As a result of such a cut, although the total number of events decreases, the relative statistical error diminishes since it is inversely correlated with the measured asymmetry. If the efficiencies of the pair events and beam intensity normalization events are assumed to be the same, then the cross section measurement in Eq. (8) reduces to counting these events separately. Denoting the number of pairs produced in perpendicular and parallel cases by p_1 and p_2, and the number of the normalization events in each case by n_1 and n_2, respectively, the measured asymmetry can be written as

$$A = \frac{p_1/n_1 - p_2/n_2}{p_1/n_1 + p_2/n_2}, \tag{10}$$

where p and n are acquired simultaneously and therefore are correlated.

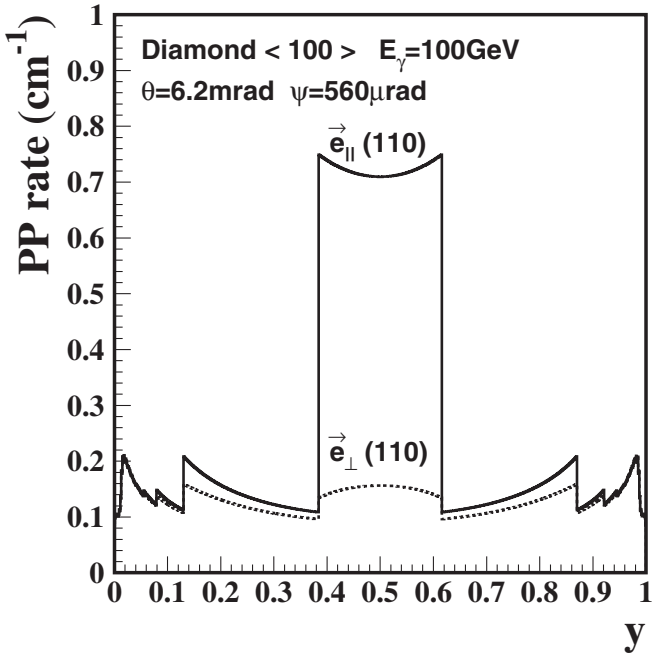

FIG. 4. Pair production rate vs the pair asymmetry, y, as defined in the text.

B. Germanium and diamond analyzer crystals

The first analyzer crystal used in the experiment was a germanium (Ge) single crystal disk with a diameter of 3 cm and a thickness of 1.0 mm. The selected orientation with respect to the incident photon beam represented a polar angle of 3.0 mrad measured from the $\langle 110 \rangle$ axis and an azimuthal angle corresponding to incidence exactly on the $(1\bar{1}0)$ plane. This configuration gave an analyzing power peaking at 90 GeV, as can be seen in Fig. 5. From the same figure, one can also see that the quasisymmetrical pair selection method delivers almost twice the analyzing power. The same single Ge crystal had also been used in a previous experiment, as reported in [45] therefore the pair-production properties of this thickness of germanium crystal are well known.

The second analyzer for this experiment was a multitile synthetic diamond crystal target with an incident photon beam orientation with respect to the crystal of 6.2 mrad from the $\langle 100 \rangle$ axis and 560 μrad from the (110) plane.

The major advantage of using diamond in the analyzer role are its high pair yield, high analyzing power (see Fig. 5), and radiation hardness. The photon beam dimensions of this experiment implied that one would need a diamond with an area of about 20 mm $\times$ 20 mm. A crystal thickness of 4 mm was a fair compromise between requirements of the figure of merit (FOM) for a diamond analyzer and the costs of the material. These requirements were realized by developing a composite target comprising of four synthetic type Ib diamonds [46–48] of dimensions $(8 \times 8 \times 4)$ mm^3 arranged in a square lattice as seen in Fig. 6.

Once beam was available, the fine alignment was performed (and indeed regularly controlled during the experiment). A narrow electron beam was directed onto the crystal, and data was collected using the minimum bias trigger (see Sec. IV A). A scan of the incident angular phase space between the beam and the crystal was performed by programming the motion of the crystal mounted in the goniometers. The crystallographic axes and planes could be identified as positions in this phase space where the coherent enhancements (or reductions) of a radiation phenomenon in relation to the corresponded incoherent cross section occurred. This would be observed in an appropriate detector.

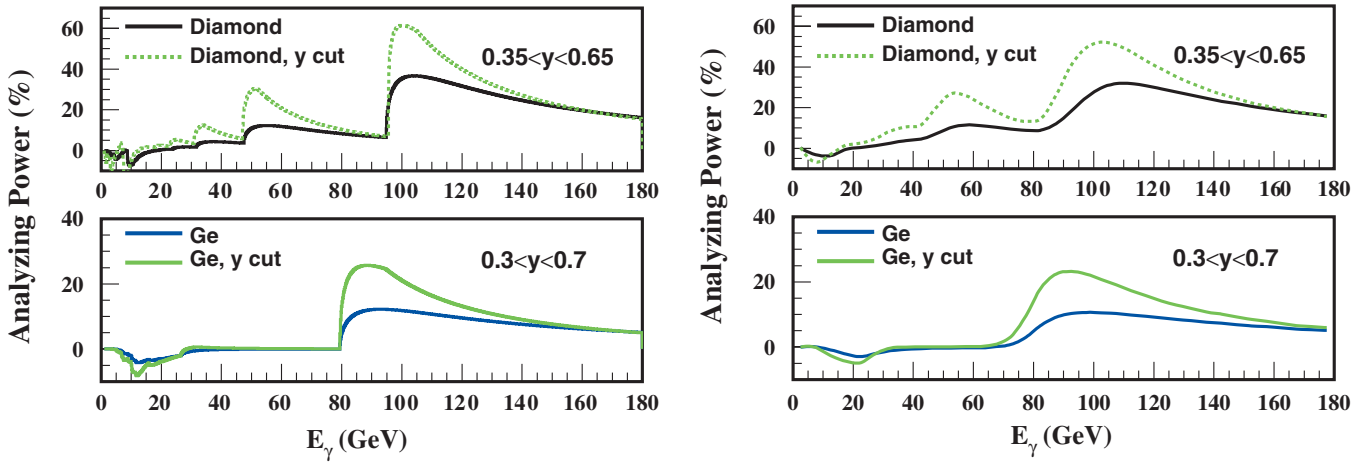

FIG. 5. (Color) Analyzing power of different single crystals, for an ideal e^- beam without any angular divergences (left) and for the actual e^- beam conditions (right).

The radiator crystal was therefore aligned exploiting the physics of bremsstrahlung from the electron beam as observed in the lead glass calorimeter. On the other hand, the analyzer crystal was aligned by observing pair production by the photon beam generated in the radiator crystal as observed in the multiplicity counter.

C. Conversion of linear to circular polarization

The second section of the experiment tested the feasibility of producing circularly polarized photon beams in proton accelerators using the extracted unpolarized high-energy electron beams [for example, with energies of up to 250 GeV (CERN) and 125 GeV (FNAL) [49,50]]. These unpolarized electron beams can produce linearly polarized photons via CB radiation in an aligned single crystal. One can transform the initial linear polarization into circular polarization by using the birefringent properties of aligned crystals. The above-mentioned method was first proposed by Cabibbo and collaborators in the 1960s [51], and later the numerical calculations were done in terms of CPP theory [18] to obtain the optimal thicknesses for various cubic crystals. To perform the experimental investigation, a consecutive arrangement of three aligned single crystals was used. The first crystal acted as a radiator to produce a linearly polarized photon beam, the second crystal acted as a quarter wave plate to convert the linear polarization into circular polarization, and the last crystal acted as an analyzer to measure the change in the linear polarization of the photon beam. The three-crystal scheme used is shown in Fig. 7.

The linearly polarized photon beam was produced by CB radiation from electrons in an aligned Si ⟨100⟩ single crystal (radiator), as already described above (Sec. II A). For the conversion of the linear polarization into circular polarization an aligned Si ⟨100⟩ crystal was used (quarter wave plate). Finally, the resulting polarization of photon beam was measured in an aligned Ge ⟨110⟩ crystal (analyzer), also as discussed above (Sec. III A).

When a high-energy photon beam propagates through a medium, the main process by which the photons are absorbed is e^+e^- pair production. When photons propagate through an aligned crystal at small incident angles with respect to a crystal axis and/or a crystal plane, a coherent

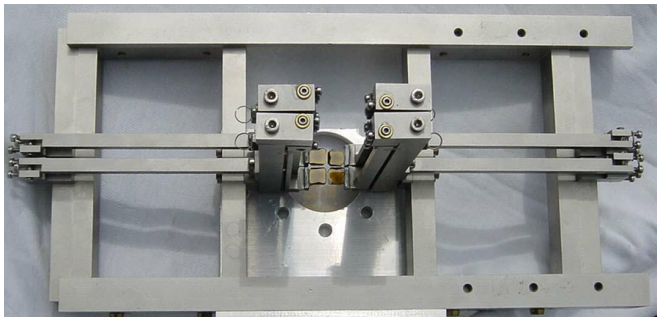

FIG. 6. (Color) The diamond analyzer target consists of synthetic diamond tiles and the aluminum holder frame.

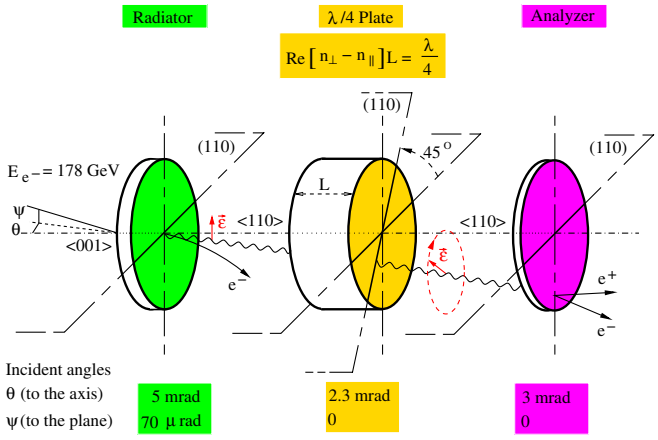

FIG. 7. (Color) Three crystal scheme.

enhancement of the PP is manifested (CPP). The cross section for the CPP process depends on the direction of the linear polarization of the photon beam with respect to the crystal axis and to the photon momentum (reaction plane) as shown in Fig. 7. Generally speaking, one can represent the linear polarization of the photon beam as a superposition of two beams with polarization directions parallel and perpendicular to the reaction plane containing the photon momentum $\boldsymbol{k}$ and the crystallographic axis. In this case, the photon polarization vector $\boldsymbol{e}$ will be the combination of two unit vectors, $\boldsymbol{t}$ and $\boldsymbol{y}$, parallel and perpendicular to the reaction plane, respectively:

$$\boldsymbol{e} = e_{\parallel}\boldsymbol{t} + e_{\perp}\boldsymbol{y}. \tag{11}$$

The components of the polarization vector before and after the crystal of thickness, L, are related by a 2×2 matrix [51,52]:

$$\begin{pmatrix} e_{\parallel}(L) \\ e_{\perp}(L) \end{pmatrix} = \begin{pmatrix} \exp[in_{\parallel}E_{\gamma}L] & 0 \\ 0 & \exp[in_{\perp}E_{\gamma}L] \end{pmatrix} \begin{pmatrix} e_{\parallel}(0) \\ e_{\perp}(0) \end{pmatrix},$$

where $E_{\gamma} = |\boldsymbol{k}|$ ($\hbar = c = 1$) is the energy of the incident photon and the $n_{\parallel}$ and $n_{\perp}$ are complex quantities analogous to the index of refraction. The imaginary part of the index of refraction is connected with the photon absorption cross section, while the real part can be derived from the imaginary part using dispersion relations [51]. The crystal can act as a quarter wave plate, if the real part of the relative phases of the two components of the waves parallel and perpendicular to the reaction plane is changed by $\pi/2$ after transmission of the photon. Thus, the crystal will be able to transform the linear polarization of the photon beam into circular polarization at the matching thickness:

$$L = \frac{2}{\pi}\frac{1}{E_{\gamma}\,\mathrm{Re}(n_{\perp} - n_{\parallel})}. \tag{12}$$

The polarization is expressed again as in Sec. III A. The photon beam intensity and Stokes parameters after the quarter wave plate with the thickness L can be derived from the following formulas [12]:

$$\begin{aligned} N(L) &= N(0)[\cosh aL + \eta_1 \sinh aL]\exp(-WL), \\ \eta_1(L) &= \frac{\sinh aL + \eta_1(0)\cosh aL}{\cosh aL + \eta_1(0)\sinh aL}, \\ \eta_2(L) &= -\frac{\eta_3(0)\sin bL - \eta_2(0)\cos bL}{\cosh aL + \eta_1(0)\sinh aL}, \\ \eta_3(L) &= -\frac{\eta_3(0)\cos bL + \eta_2(0)\sin bL}{\cosh aL + \eta_1(0)\sinh aL}, \end{aligned} \tag{13}$$

with

$$\begin{aligned} a &= E_{\gamma}\,\mathrm{Im}(n_{\perp} - n_{\parallel}) = \tfrac{1}{2}(W_{\parallel} - W_{\perp}), \\ b &= E_{\gamma}\,\mathrm{Re}(n_{\perp} - n_{\parallel}), \qquad W = \tfrac{1}{2}(W_{\parallel} + W_{\perp}), \end{aligned} \tag{14}$$

where $W_{\parallel}$ and $W_{\perp}$ are the pair-production probabilities per unit path length for photons polarized parallel or perpendicular to the reaction plane, respectively.

As follows from Eq. (13), the component of the linear polarization in the direction of 45° to the reaction plane of the quarter wave crystal is transformed into circular polarization [12]. Therefore the quarter wave plate should be rotated by 45° with respect to the polar plane of the photon beam to have the optimal transformation of the polarization. In this case the linear polarization component η_3, which was defined as the one parallel or perpendicular to the reaction plane of the radiator, represents a component of the linear polarization in the direction of 45° to the reaction plane of the quarter wave plate Eq. (13).

As follows from Eq. (13), the total polarization of the photon beam before and after the quarter wave crystal are connected by the relation

$$P^2_{\mathrm{total}}(L) = 1 + \frac{P^2_{\mathrm{total}}(0) - 1}{(\cosh aL + \eta_1(0)\sinh aL)^2}. \tag{15}$$

There is conservation of polarization if the incident photon beam is completely polarized. In a real experiment, the incident photon beam is not completely polarized, and one must seek an alternative conserved quantity. Further study of Eq. (13) reveals that the quantity

$$K \equiv \frac{\eta_2^2(\ell) + \eta_3^2(\ell)}{1 - \eta_1^2(\ell)} \tag{16}$$

is constant and conserved when a photon beam penetrates the quarter wave plate crystal [53]. This relation holds for any penetration length, ℓ, between $0 \le \ell \le L$ except in the case when $\eta_2(0) = \eta_3(0) \equiv 0$ and $\eta_1(0) = 1$. It allows the determination of the resulting circular polarization of photon beam by measuring its linear polarization before and after the quarter wave plate. Taking into account the experimental condition, i.e., the photon beam angular divergences, one can note that K is conserved with $\approx 5\%$ accuracy in the 80–110 GeV region as shown by Monte Carlo simulations.

Figure 8 shows the expected dependence of the Stokes parameters describing the photon polarization as a function of the quarter wave plate thickness, ℓ, for the surviving photons from a beam of 100 GeV. One can see that the initial total polarization is not conserved in the case of a partially polarized photon beam as expected from Eq. (15), nevertheless, the relation (15) still holds.

These calculations were carried out assuming that the Stokes parameters before the quarter wave plate had the following values: $\eta_1 = 0.01$, $\eta_2 = 0$, and $\eta_3 = 0.36$. In Fig. 8 (left), the photon beam makes an angle $\theta_0 = 2.3$ mrad with respect to the $\langle 110 \rangle$ axis and lies in the (110) plane ($\psi = 0$), while in Fig. 8 (right), the photon beam traverses the (110) plane at a small angle, $\psi = \pm 40$ μrad.

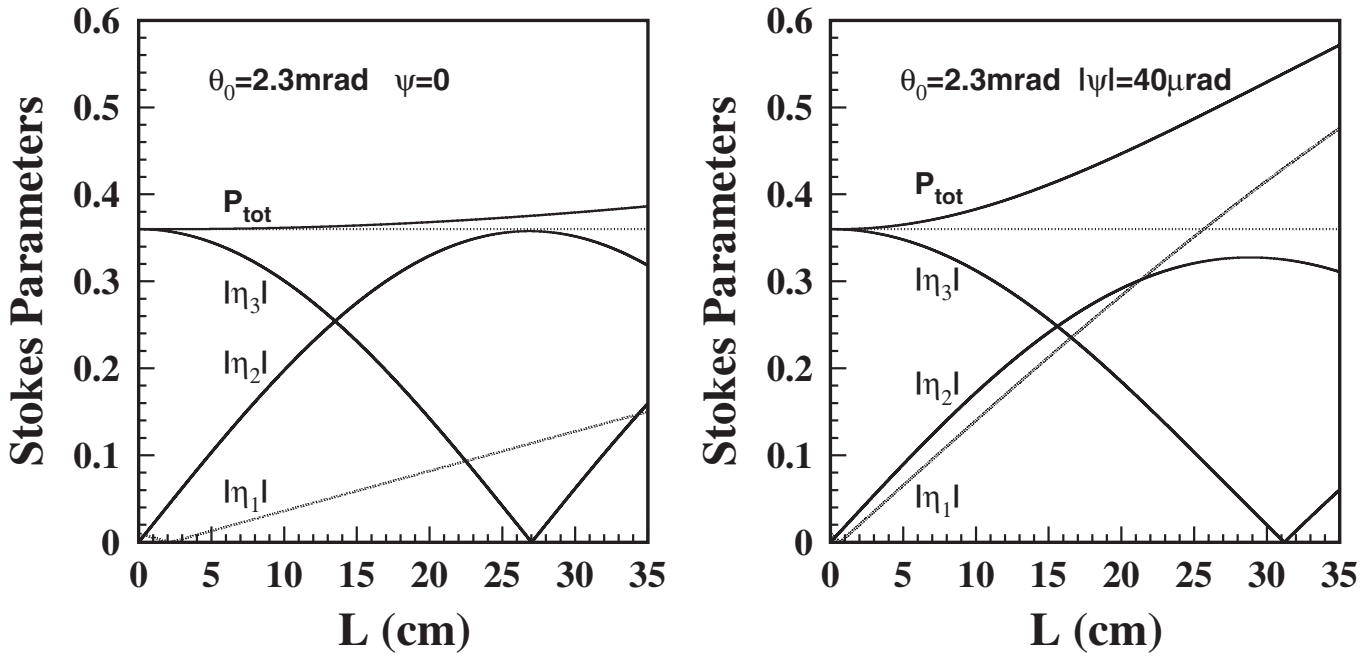

FIG. 8. (Color) Absolute values of the Stokes parameters and the total degree of polarization for a Si crystal as a function of its thickness L, for $E_\gamma = 100$ GeV linearly polarized photons. The left-hand figure and the right-hand figure are calculated using initial values for the Stokes parameters described in the text. For these conditions, the crystal also acts as polarizer generating a η_1 component.

One can see the increase in the total polarization, P_{total}, after the quarter wave plate with respect to the initial total polarization (the straight line around 0.36). This difference comes from the fact that the aligned quarter wave plate can also act as a polarizer. Therefore, the total polarization behind the quarter wave plate can be higher than the initial polarization. This increase is more pronounced in the case when the photon momentum makes a small angle of $\psi = 40$ μrad with respect to the crystal plane (Fig. 8 right). As described in Sec. IVA and as shown in Fig. 20, the final calculation takes into account the beam divergence, in both the horizontal and vertical planes.

As seen from Fig. 8, the Si crystal with a thickness of $L > 25$ cm has indeed acted as a quarter wave plate and generated a degree of circular polarization taking into account the angular divergence of the γ-beam. For these crystal thicknesses where the $\eta_3(0)$ component of the initial linear photon beam polarization will be totally transformed into the final circular component $\eta_2(L)$, only a few percent of the photons will survive. We defined a FOM, to find a compromise between the photon beam attenuation and the polarization transformation efficiency in [49], as

$$\text{FOM} = \eta_2(\ell)\sqrt{N(\ell)}. \tag{17}$$

Here $N(\ell)$ is the statistical weight of the number of surviving photons. Taking into account Eq. (17), Refs. [54–56] presented theoretical predictions showing the possibility of transforming the linear polarization of a high-energy photon beam into circular polarization in the 70–100 GeV energy range. The theoretical calculations of the energy and the orientation dependence of the indices of refraction were performed using the quasiclassical operator method and CPP formulas, respectively. In both these references, the optimum thickness for a quarter wave plate Si crystal was found to be 10 cm. The relevant geometrical parameters involved the photon beam forming an angle of 2.29 mrad from the axis (110) and the photon momentum directly in the (110) plane of Si single crystal, i.e., the angle between the photon momentum and crystal plane is $\psi = 0$. For this choice of parameters, the fraction of surviving photons is 17%–20%.

D. SOS radiation

For the production of the much enhanced yield of the SOS photons as compared to the CB photons, the first radiator crystal was adjusted to appropriate angle settings. These were a beam angle of $\theta = 0.3$ mrad to the $\langle 100 \rangle$ axis in the (110) plane of the 1.5 cm thick Si crystal which is the optimal angle for a high-energy SOS photon peak at 129 GeV (see Fig. 3) energy photon peak with a thin radiator at 125 GeV (see Fig. 3). As has been mentioned in Sec. II B, the radiation probability with a thin radiator is expected to be 20 times larger at that energy than the Bethe-Heitler (ICB) prediction for randomly oriented crystalline Si.

The polarization measurements were then performed in a similar way to those of Sec. III A for the analysis of linear polarization in CB radiation.

IV. EXPERIMENT AND ANALYSIS

The experiment was performed in the North Area of the CERN SPS, where unpolarized electron beams with energies above 100 GeV are available. We used a beam of 178 GeV electrons with angular divergence of $\sigma_{x'} = 48$ μrad and $\sigma_{y'} = 35$ μrad in the horizontal and vertical plane, respectively.

A. The setup

The experimental setup described below and shown schematically in Fig. 9 is ideally suited for detailed studies of the photon radiation and pair-production processes in aligned crystals.

The radiator system comprised of the 178 GeV unpolarized electron beam focused on the single crystal silicon radiator (XTAL1). The crystal was of cylindrical shape with a 2.5 cm radius and a 1.5 cm thickness. It was aligned using a goniometer of 2 μrad precision to obtain either CB or SOS radiation conditions, as required. Upstream drift chambers (dch1up-2up) allowed tracking of the incoming beam with an angular precision of 4 μrad to define the position of incident electron in the incident angle phase space. The drift chambers had an active area of (15×15) cm^2 divided into six cells in both horizontal and vertical planes. A double sense wire configuration removed the directional hit ambiguity. The exit angles of the electron emerging from the radiator crystal was recorded by two tracking chambers (dch2up and dwc3). This allowed the measurement of electron multiple scattering angle inside the crystal. The dwc3 is a multiwire proportional chamber [57] with an active area of about (10×10) cm^2 and a resolution of 200 μm.

The photon tagging system consisted of a dipole magnet (Bend8) capable of a maximum beam rigidity of 4.053 Tm and a special drift chamber (dch0) with no active horizontal cells. This constituted an upstream spectrometer which measured the energy of the spent electron (with an acceptance of 10–90% of the incident energy). A beam dump protected the rest of the system from background effects arising from the spent electron.

The polarization analyzer system followed next. After passing a helium bag of length 9.65 m to reduce the multiple scattering, the remaining photon beam impinged on the analyzer crystal aligned with a goniometer of 20 μrad precision. The number of charged particles coming out of the analyzer crystal was counted both by a scintillator (S11) for fast triggering and a solid state detector (not shown) for offline analysis. The S11 scintillator was used to detect the photon conversion into e^+e^- pairs at the analyzer and it measured the number of charged particles seen right after the crystal analyzer. For the analysis, we only used events with 2MIPs in S11, as a signature for PP events [a minimum ionizing particle (MIP) leaves a well defined energy in the S11 scintillator, so the selection is for e^+-e^- events]. The photons which did not scatter or interact and the electron positron pairs created by the interacting photons continued into a magnetic spectrometer.

The pair-spectrometer system was introduced next to measure the energy spectrum of the photon beam in a multiphoton environment. The dipole analyzer magnet (Trim6) of the spectrometer was capable of a maximum beam rigidity of 0.53 Tm. The tracking elements upstream of the magnet consisted of one drift chamber (dch1) for the Ge analyzer and two drift chambers (dch05 and dch1) for the diamond analyzer. There were two drift chambers (dch2,dch3) downstream of the magnet. The drift chambers measured the horizontal and vertical positions of the passing charged particles with a precision of 100 μm yielding a spectrometer resolution of $\sigma_p/p^2 = 0.0012$ with p in units of GeV/c.

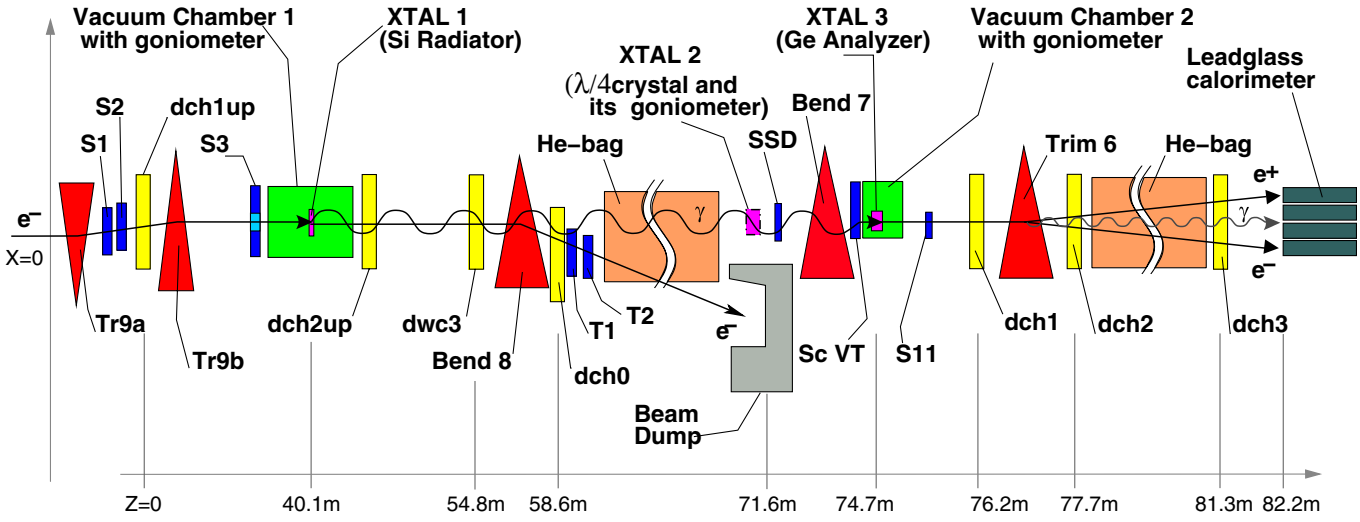

FIG. 9. (Color) The experimental setup.

The calorimeter system measured E_γ^{tot}, the total radiated energy. This was done in a 12-segment array lead-glass calorimeter of 24.6 radiation lengths which had a resolution of $\sigma/E = 11.5\%/\sqrt{E}$, with E in units of GeV. The central segment of this lead-glass array was used to map and align the crystals with an electron beam [43]. A more detailed description of the experimental apparatus is reported elsewhere [58,59].

Various plastic scintillators (Sn or Tn) were used to calibrate the tracking chambers and to define different physics triggers. The normalization event trigger (*norm*) consisted of the signal logic combination $S1 \cdot S2 \cdot \overline{S3}$ to ensure that an electron is incident on the radiator crystal. The scintillator Sc VT rejects radiation events coming from the conversion of the tagged photon beam upstream of the crystal analyzer. This trigger is also the minimum bias trigger as it does not favor any energy, angle, or interaction process, but is expected to enter the experimental setup correctly. The radiation event trigger (*rad*) could then be defined as the signal logic combination $norm \cdot (T1.or.T2) \cdot \overline{VT}$ indicating that the incoming electron has radiated and has been successfully taken out of the photon section of the beam line. The pair event trigger (*pair*) was constructed as the signal logic combination $rad \cdot S11$ to select the events for which at least one e^+e^- pair was created inside the analyzer crystal.

FIG. 10. (Color) Birefringent (quarter wave plate) Si crystal and goniometer.

The three different experimental measurements described in this paper customized the experimental setup as follows: (i) The measurement of the CPP cross section by linearly polarized photons on aligned crystals (birefringent effects in CPP) was performed using only the radiator and analyzer crystals. Both germanium and diamond analyzers were investigated. This measurement also established the new aligned crystal polarimetry technique. (ii) The investigation of the conversion of linear polarization to circular polarization for the CB photons necessitated the inclusion of an additional crystal, denoted as the quarter wave. The crystal polarimetry technique was extended to quantify circular polarization as well. The magnet B7 served as a sweeping magnet of the particles produced by electromagnetic showers in the quarter wave plate. A solid state detector SSD (500 μm thick Si crystal, 5×5 cm^2) was placed right after the quarter wave crystal during dedicated runs in order to study the shower development. (iii) The measurement of the polarization of SOS radiation was done without the quarter wave plate in the system, and in this case the radiator was configured to generate SOS radiation.

The case of the deployment of the quarter wave plate needs additional explanation. A third goniometer controlled the 10 cm thick Si $\langle 110 \rangle$ crystal, that served as the quarter wave plate. It was located after the He-bag. A photograph of the quarter wave plate and the goniometer is shown in Fig. 10. The orientation of this crystal relative to the photon beam was already discussed in Sec. III C (see Table I for a summary of the crystal parameters).

The axis of the Si crystal was carefully prealigned with respect to the axis of the azimuthal annular stage that was subsequently mounted into the main goniometer. This prealignment procedure was carried out at ESRF, Grenoble. A schematic of the alignment setup and the results are shown in Fig. 11. An x-ray reflection satisfying the Bragg condition was used to monitor the orientation of the (110) crystallographic plane which is perpendicular to the $\langle 110 \rangle$ axis. The crystal was rolled in steps using the azimuthal goniometer stage (ϕ angle rotation). The $\langle 110 \rangle$ crystallographic axis was slightly misaligned with the crystal physical longitudinal axis and therefore also initially slightly misaligned with the azimuthal annular stage longitudinal axis. At each azimuthal step, the Bragg condition had therefore to be recovered by adjustments to the angle of crystal face using a second goniometer (θ angle rotation). The Bragg condition was recognized by locating the two points at half maximum of the Bragg peak. From a plot of the adjustment angle θ for each step in the roll angle ϕ of the azimuthal goniometer, the precise offset angles between the azimuthal goniometer longitudinal axis and

TABLE I. Description of the angle settings for the quarter wave plate setup, where θ_0 is the angle between the photon momentum and crystal axis, ψ is the angle between the photon momentum and the indicated crystal plane, and ϕ is the azimuthal angle of the quarter wave plate relative to the radiator.

Crystal type	Purpose	Axes and planes	Orientation	Thickness
Si	Radiator	⟨001⟩, (110)	$\theta_0 = 5$ mrad, $\psi_{(110)} = 70$ μrad	1.5 cm
Si	Quarter wave plate	⟨110⟩, (110)	$\theta_0 = 2.3$ mrad, $\psi_{(110)} = 0$	10 cm
Ge	Analyzer	⟨110⟩, (110)	$\theta_0 = 3$ mrad, $\psi_{(110)} = 0$	1 mm
	η_1 measurement		$\phi = \pi/4, 3\pi/4$	
	η_3 measurement		$\phi = 0, \pi/2$	

the ⟨110⟩ crystallographic axis could be obtained. As the thick Si crystal was mounted in the azimuthal stage by adjustment screws, the ⟨110⟩ crystallographic axis could then be brought into coincidence with the longitudinal axis of the azimuthal goniometer.

The data acquisition system consisted of personal computers running the Linux operating system and using in-house developed software to access the VME and CAMAC readout crates containing the digitization modules. The chamber signals were read out by VME TDC modules (Caen v767) with 1 ns resolution. The scintillator and calorimeter signals were read out with CAMAC ADC modules (LRS 2249) with 0.3 pC resolution. The raw data was then stored on digital linear tape for offline analysis. The Trigger and DAQ Systems of the experiment are described in more detail elsewhere [60].

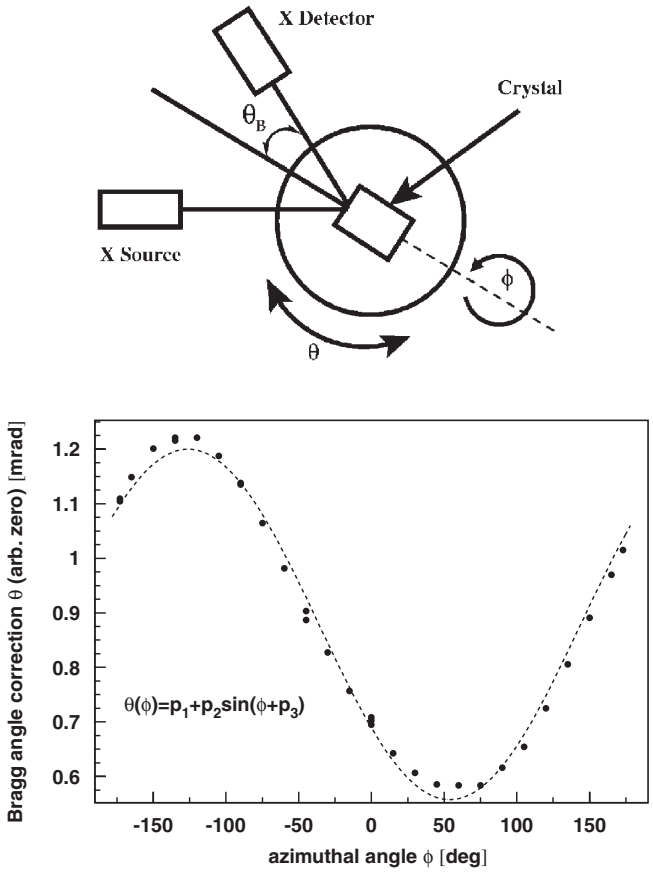

FIG. 11. Schematic setup (top) and measurements of the Bragg peak adjustment angle θ as a function of the azimuthal rotation angle ϕ (bottom) for the annular stage alignment of the quarter wave plate crystal with x rays.

B. Analysis

The first step in the offline analysis was the beam quality cuts, which ensured the consistency of various trigger ratios and the initial beam position and angles during data taking. Next, to facilitate comparison of the experimental results with theoretical predictions, the angular divergence of the electron beam was restricted to $\pm 3\sigma$ from its mean. Determination of the electron trajectory and its impact point on the radiator were essential for fiducial volume requirements. The radiated photons were taken to follow the direction of the initial electron. This is accurate to $1/\gamma \approx 5$ μrad for 100 GeV electrons. To reconstruct the single photon energy in each event, only events where a single electron positron pair was manifest in the spectrometer volume with the pair energy being the same as the photon energy were selected. This subset of pair events was further classified into families according to the number of hits on the drift chambers of the spectrometer. In our nomenclature, "122-type" events are clearly the cleanest ones with one hit in the first upstream chamber, and two in both the second and third downstream drift chambers. The resulting pair-production vertex was required to be in the fiducial volume of the analyzer crystal. For the case of the diamond analyzer, the additional drift chamber on the upstream side ensured a better vertex reconstruction. This in turn allowed us to veto the intertile events as well as the ones coming from the misaligned tile. Quality assessment of the pair search program was performed by a GEANT based Monte Carlo program. This program simulated the effects of the detector geometry to understand the precision and efficiency of the reconstruction algorithm for each event family. Further details of the analysis are recorded in Ref. [61].

During the data taking, to obtain the parallel and perpendicular configurations, the angular settings of the radiator crystal (hence the direction of linear polarization of the photon beam) were kept constant. Only the analyzer crystal was rotated in a rolling motion around its symmetry

TABLE II. Different material and angular settings for the analyzer crystal used to measure the linear polarization components. The angle ϕ is defined in the caption of Table I.

Analyzer orientation (ϕ)	Analyzer type	Measured polarization component
$0, \frac{\pi}{2}, \pi, \frac{3\pi}{2}$	Ge	η_3
$\frac{\pi}{4}, \frac{3\pi}{4}, \frac{5\pi}{4}, \frac{7\pi}{4}$	Ge	η_1
$0, \frac{\pi}{2}$	Diamond	η_3

axis. Therefore to measure the magnitude of the η_3 (η_1) component of the polarization, analyzer orientations separated by $\pi/2$ starting from 0 ($\pi/4$) were compared. To reduce the systematic errors (especially in the case of the Ge crystal where the analyzing power is smaller), all relevant angles on the analyzer crystal were utilized for polarization measurements, as presented in Table II. Other sources of systematic errors were the uncertainty in the crystal angles, the photon tagging, and the pair reconstruction efficiencies obtained from Monte Carlo studies.

C. CB validation

The angular settings of the radiator crystal were verified by inference from the data. The single photon intensity spectrum presented in Fig. 12 contains two different event selections superimposed on the Monte Carlo prediction. The geometrical acceptance of the spectrometer for 122-type events, named after their reconstruction in drift chambers, has a relatively high threshold of 30 GeV, as seen from the Fig. 12. The large number of low energy photons

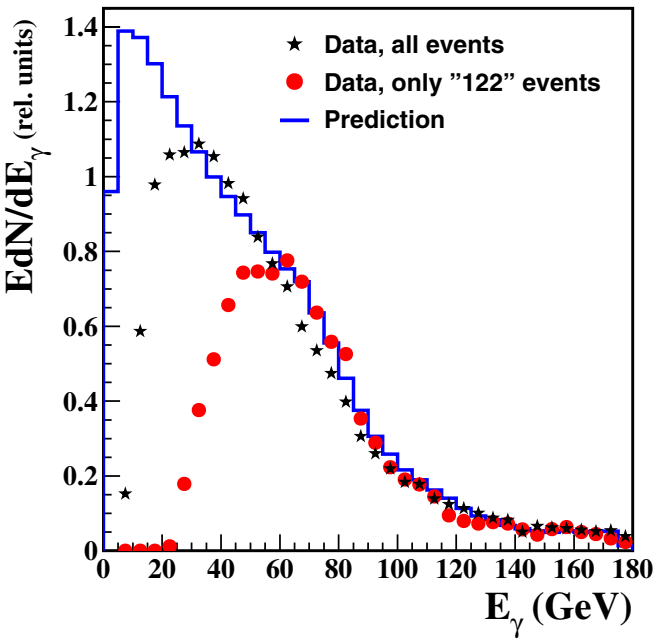

FIG. 12. (Color) Monte Carlo predictions for the single photon spectrum, compared with data using all events (stars) and only 122-type events (circles).

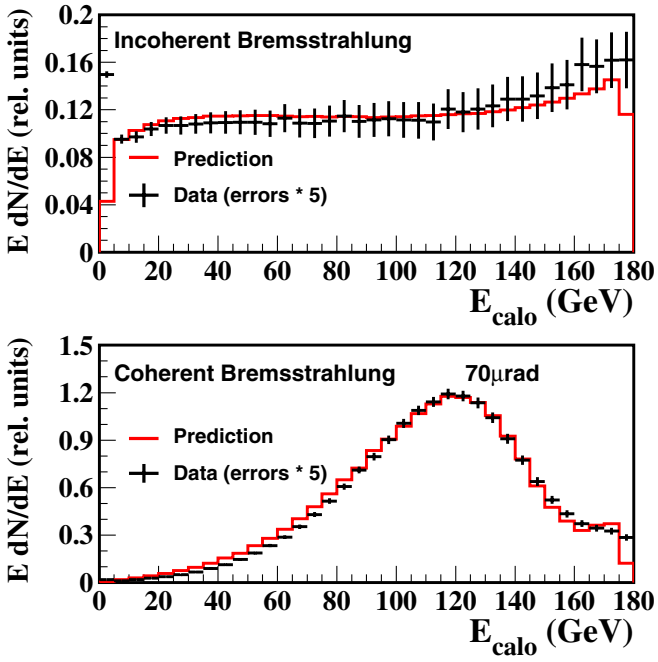

FIG. 13. (Color) Power spectrum for incoherent (top) and for coherent bremsstrahlung (bottom) as a function of the total energy E_{calo} detected in the calorimeter. Vertical axis: Power (relative units). The statistical errors on the data are enhanced by a factor of 5 to increase visibility.

is due to the thickness of the target (1.5 cm) and the small angle of incidence (70 μrad).

An independent method of verifying the CB settings is looking at the total electromagnetic radiation from the

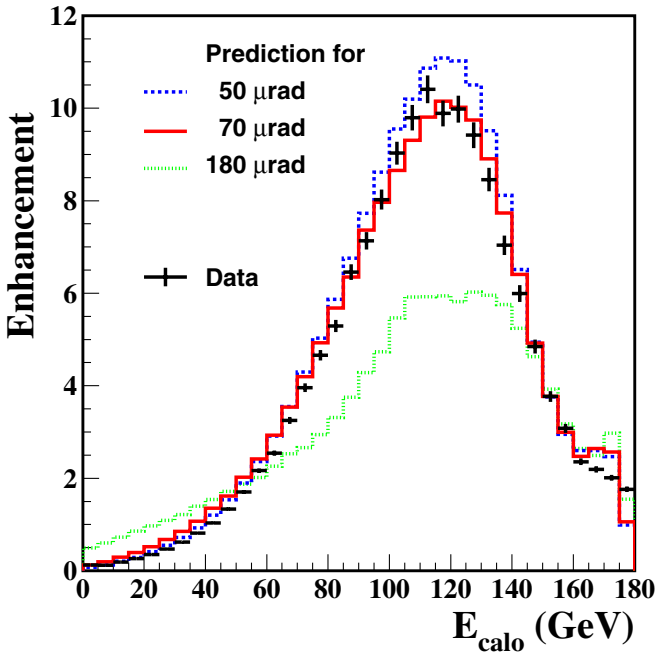

FIG. 14. (Color) Enhancement of CB radiation data compared to Monte Carlo predictions. Note the sensitivity of the cross section to small changes in the angular setting of the crystal.

radiator crystal. Figure 13 shows the total power spectrum (E dN/dE) as a function of the energy measured in the calorimeter for the radiator crystal not aligned [Fig. 13(top)] and aligned [Fig. 13(bottom)]. In terms of the radiation intensity spectrum, an unaligned crystal is identical to an amorphous material. This radiation is called ICB and it can be approximated by the familiar Bethe-Heitler formula [62]. The increase in the CB radiation intensity spectrum is usually reported with respect to the IB spectrum. This ratio, called the "enhancement," is presented in Fig. 14 together with Monte Carlo prediction for CB angle at 70 μrad. The agreement of the data with the enhancement prediction is remarkable. The offline analysis could therefore be used to monitor the angular settings of the radiator in time steps, to ensure the crystal angular settings did not drift during the measurement.

V. RESULTS

A. Birefringence in CPP and a new crystal polarimetry

The orientation of the radiator crystal could be accurately determined by comparison of the predicted and measured CB enhancement (Fig. 14). The predicted and measured asymmetries for both linear polarization components, η_1 and η_3, could then be confidently compared. Using all events, as well as events passing the quasisymmetrical pairs selection criteria, we see that, as expected, the asymmetry in Fig. 15 is consistent with zero yielding a vanishingly small η_1 component of the polarization.

The measured asymmetry in the induced polarization direction (η_3) is presented in Fig. 16 without and with the y-cut using the Ge analyzer crystal. The solid line represents the Monte Carlo predictions without any smearing effects considered in the spectrometer. The lower plot represents the increase in the asymmetry due to quasisymmetrical pairs together with the statistical error associated with this increase. It thus confirms the nonstatistical source of the asymmetry increase in the 70–110 GeV range. The same polarization as measured by the diamond analyzer is given in Fig. 17. The top and middle plots show again the asymmetry measurements as compared to the Monte Carlo predictions without any smearing, and the lower plot shows the increase in the asymmetry due to the y-cut. Comparing

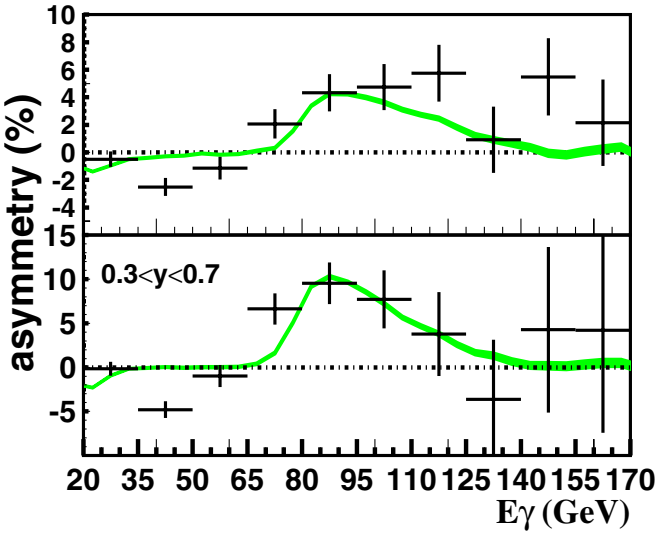

FIG. 16. (Color) Asymmetry to determine the η_3 component of the CB photon polarization with the Ge analyzer. Measurements *without* (top) and *with* (bottom) the quasisymmetrical pair selection at roll angles $0 + \pi$ are compared to those at roll angles $\pi/2 + 3\pi/2$.

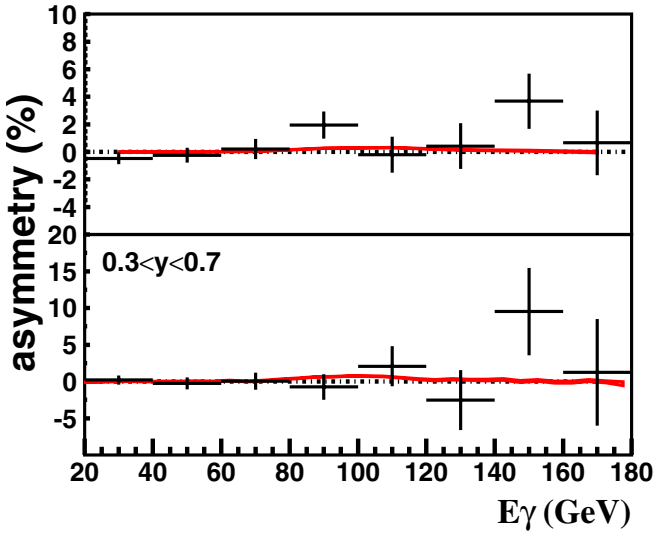

FIG. 15. (Color) Asymmetry to determine the η_1 component of the photon polarization with the Ge analyzer. The data at roll angles $\pi/4 + 5\pi/4$ are compared to $3\pi/4 + 7\pi/4$ *without* (top) and *with* (bottom) the quasisymmetrical pair selection.

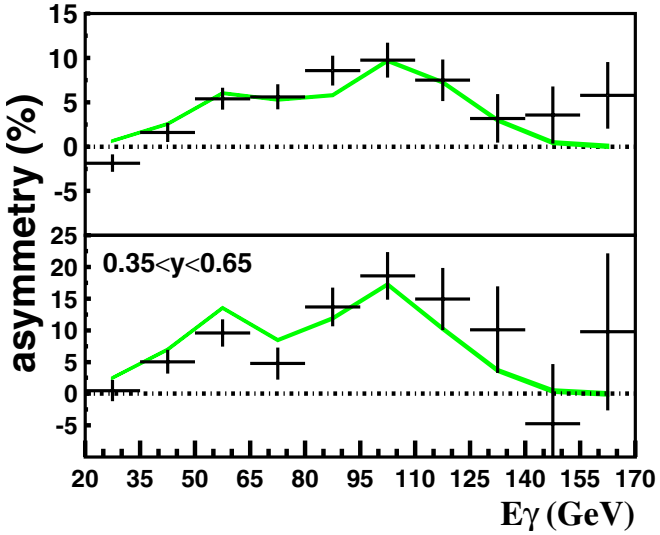

FIG. 17. (Color) Asymmetry measurements *without* (top) and *with* (bottom) the quasisymmetrical pair selection to determine η_3 component of the photon polarization with the *diamond* analyzer (cf. Table II).

Figs. 16 and 17, we conclude that the multitile synthetic diamond crystal is a better choice than the Ge crystal as an analyzer, since for the same photon polarization the former yields a larger asymmetry and thus enables a more precise measurement. The diamond analyzer also allowed the measurement of the photon polarization in the 30–70 GeV range, since it has some, albeit small, analyzing power at these energies.

The theoretical predictions are based both on the calculation of the energy dependent polarization of photons produced by coherent bremsstrahlung and the polarization dependence of coherent pair production, also as a function of incident energy. Thus, the polarization sensitive versions of both CB and CPP are needed together in the theoretical calculation that predicts the measured asymmetry. The theoretical calculation combines the coherent and quasiclassical theories of radiation and pair production, in a Monte Carlo approach that can describe real beams with finite divergence. The agreement of this combined theory with the measured data is remarkable. It is clear that for the energy range of 30–170 GeV and the incident angle phase space of this study that the theory is sufficiently reliable and well understood to support the development of applications of crystals as polarimetry devices. The calculation of the resolving power [R in Eq. (8)] is therefore reliable for the energy and angle regimes discussed in the introduction. The asymmetry measurements therefore correspond to a measurement of the induced polarization for CB for η_3 shown in Fig. 2. This has a maximum of 57% at 70 GeV.

B. Conversion of linear to circular polarization

In this part of the experiment, the quarter wave plate crystal was introduced between the *radiator* and analyzer crystals. The linear polarization measurements mentioned in the previous section were extended to allow the measurement of circular polarization. This measurement is related to a reduction in linear polarization and the conservation of polarization. The theoretical background was described in Sec. III C. It is noted that the expected and measured single photon spectrum for the chosen CB parameters for the radiator as shown in Fig. 12 are in good agreement. The expected polarization for the same set of parameters has already been given in Fig. 2 as a function of the single photon energy. As shown in the previous section, this polarization has been confirmed for the η_1 and η_3 components. This indicates that the linearly polarized CB photon beam is well understood.

Any change in the single photon spectrum after adding the quarter wave crystal will reflect how the incoming photons are absorbed or transformed by it. As η_1 was found to be consistent with zero before the quarter wave crystal, any nonzero value observed after it is a reflection of birefringent effects of the crystal.

Detailed theoretical calculations and simulations have been done to choose the crystal type, orientation, and optimal thickness for the quarter wave crystal, leading to the choice of a 10 cm thick Si crystal as discussed above. The analysis took into account the real experimental pa-

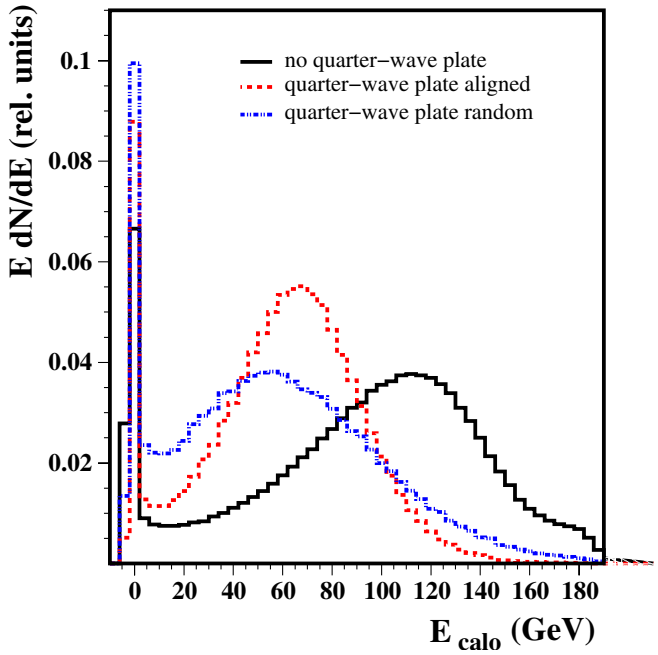

FIG. 18. (Color) Power spectrum of the photon beam measured in the calorimeter. Without the quarter wave plate crystal, the predicted CB spectrum is observed (solid line). With the aligned quarter wave plate inserted, the spectrum shifts to lower energies (dashed line). With the quarter wave plate in random orientation, we see more spread in the shifted spectrum.

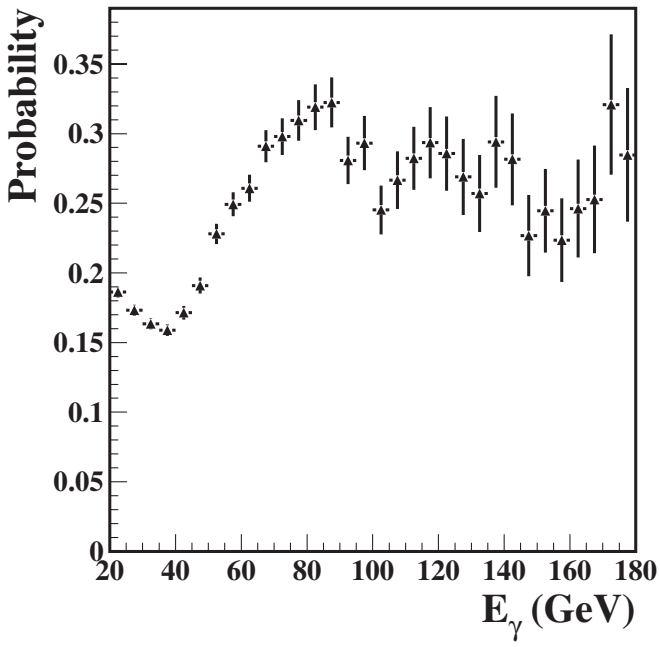

FIG. 19. Absorption probability found from the ratio of the single photon spectrum for the data with and without the quarter wave crystal.

rameters including the angular spread of the incident photon beam, the generation of secondary particles, multiple Coulomb scattering, and all particles produced by electromagnetic showers were also taken into account. In the simulation we assume the angular spread of the photons with energies between 70–100 GeV to be ~60 μrad and ~45 μrad in horizontal and vertical planes, respectively, as measured from the data. The calculations also include the polarization transformation part for the surviving photon beam, resulting in elliptical polarization.

Figure 18 shows the photon beam power spectrum measured with the lead glass electromagnetic calorimeter. The calorimeter sees all the surviving photons radiated by the parent electron. By comparing the spectrum with the quarter wave crystal at random and/or aligned with the case in which there is no quarter wave crystal, we can see that the quarter wave plate consumes a significant amount of the beam. This causes the peak energy of the pileup spectrum to be reduced by at least 50 GeV. However, it is also clear that the energy of the photons absorbed by the quarter wave crystal depends on its alignment condition.

As already mentioned in Sec. III C, the prediction is that only 17%–20% of the photons are expected to survive in the energy region of interest. This is confirmed by the data, see Fig. 19. In addition, it is clear that the survival probability is also energy dependent as expected.

Another consequence of adding the quarter wave crystal is a significant increase in the photon multiplicity of an event. For example, we expect an average multiplicity of three photons per electron for the nominal radiator settings. By analyzing the correlation between the calorimeter spectrum and the single photon spectrum, we can conclude that the majority of these photons have energies <5 GeV, and that the calorimeter events at high energies are dominated by a single high-energy photon and not due to the pileup of many low energy photons. As a consequence, the measure-

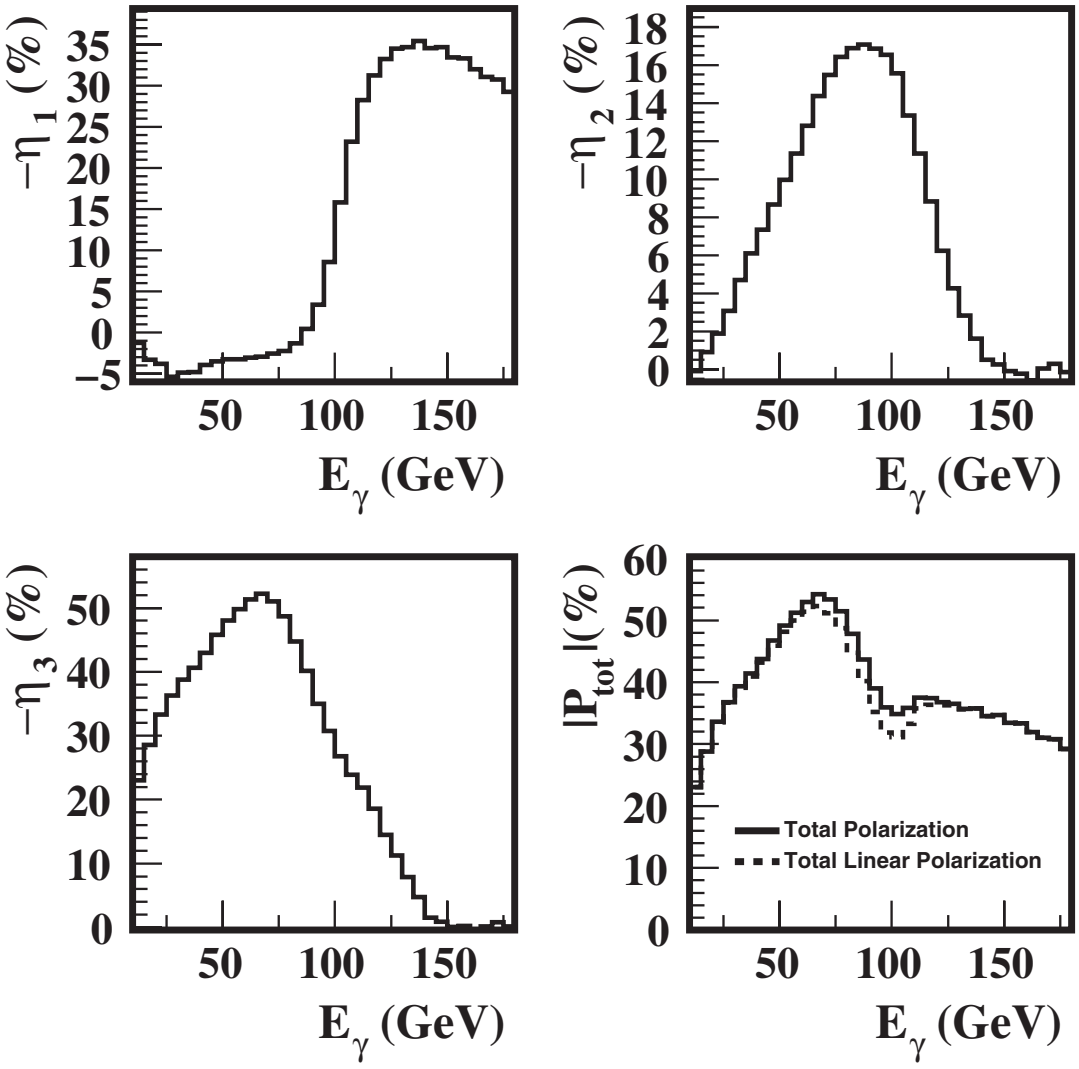

FIG. 20. Stokes parameters after the quarter wave crystal, assuming as input the values given in Fig. 2.

ment of the Stokes parameters in the high-energy range can be performed by measuring the asymmetry using either the calorimeter or the pair spectrometer.

The expected Stokes parameters and the total polarization of the photons after the quarter wave crystal are given in Fig. 20. As shown, the expected value of the η_3 Stokes parameter decreases from 36% to 30% around 100 GeV. This difference should be seen in the PP asymmetry. The expected degree of circular polarization is of the order of $\sim$16% at the same energy. In Fig. 20, we expect an interesting increase of up to a factor of 7 for the η_1 Stokes parameter in the same energy region. This phenomenon was also predicted by Cabibbo [63]; the unpolarized photon beam traversing the aligned crystal becomes linearly polarized. This follows from the fact that the high-energy photons are mainly affected by the PP process. This cross section depends on the polarization direction of the photons with respect to the plane passing through the crystal axis and the photon momentum (polarization plane). Thus, the photon beam penetrating the oriented single crystal feels the anisotropy of the medium. For the experimental verification of this phenomenon with photon beams at energies of 9.5 and 16 GeV, see [64,65]. In the high-energy region $>$100 GeV, the difference between the PP cross sections parallel and perpendicular to the polarization plane is large. Since the photon beam can be regarded as a combination of two independent beams polarized parallel and perpendicular with respect to the reaction plane, one of the components will be absorbed to a greater degree than the other one, and the remaining beam becomes partially linearly polarized.

The measured asymmetries using the calorimeter are given in Fig. 21 and again using the pair spectrometer in Fig. 22. In order to reduce systematic uncertainties, the angular settings of the radiator crystal (hence the direction of linear polarization of photon beam) were kept constant, and only the analyzer crystal was rolled around its symmetry axis to obtain the parallel and perpendicular configurations. Therefore, to measure the polarization of the η_3 (η_1) component, the asymmetry between the 0 ($\pi/4$) and $\pi/2$ ($3\pi/4$) analyzer orientations was used.

As shown in these figures, the measured asymmetries are in agreement with the predicted polarization for the chosen Ge analyzer crystal setting [66]. For the Stokes parameter η_3, the measured asymmetry after the quarter wave crystal is about $2.9 \pm 0.7\%$ in the energy range between 80–100 GeV. The estimated analyzing power R for the Ge analyzer in the same energy range is about 10% [66]. Using Eq. (8), one can estimate the measured Stokes parameter η_3 after the quarter wave crystal. Thus, the measured Stokes parameter is $\eta_3 = 28 \pm 7\%$ (see Fig. 20). For the Stokes parameter η_3, the measured asymmetry without the quarter wave crystal in the same energy range was found to be $4.7 \pm 1.7\%$ (see [66]). This corresponds to a measured value of $\eta_3 = 44 \pm 11\%$, which is also consistent with the theoretically expected value of η_3, see Fig. 2.

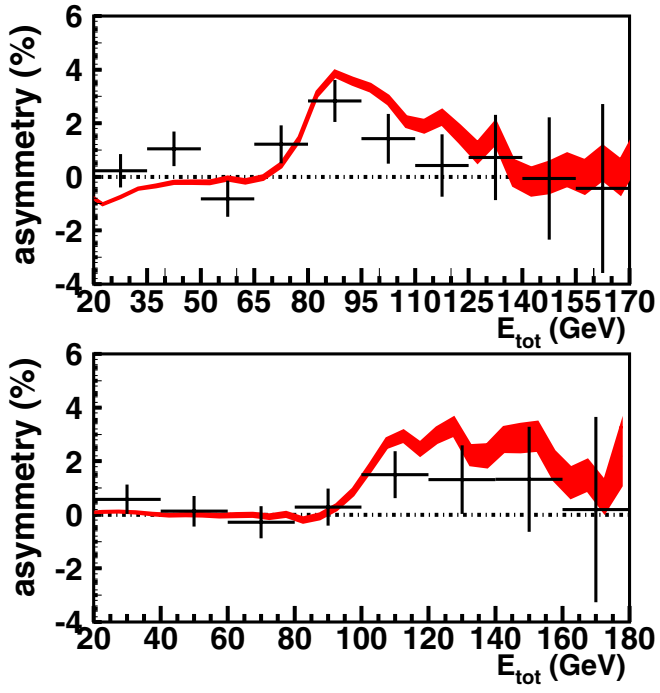

FIG. 21. (Color) Asymmetry measured with the calorimeter. The results reflects the changes in η_3 (top) and generation of η_1 (bottom) due to the presence of the quarter wave crystal.

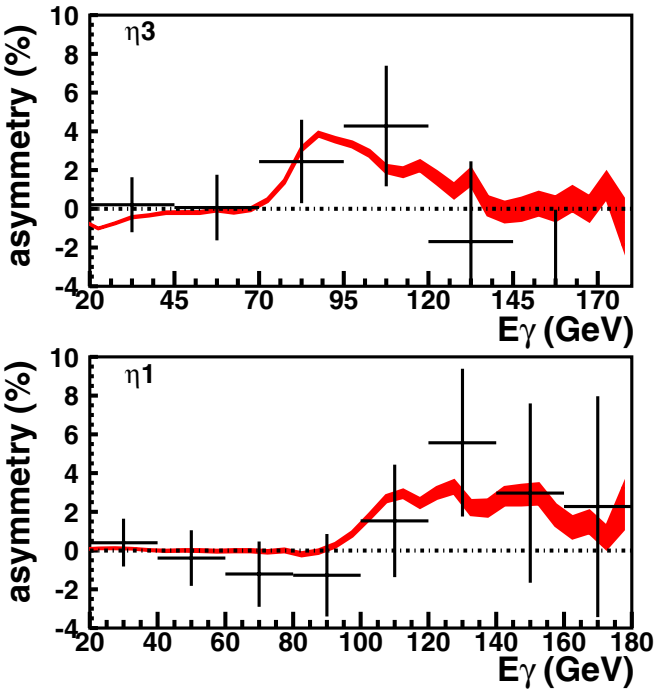

FIG. 22. (Color) Asymmetry measured with the Ge analyzer (top) and the pair spectrometer (bottom). The data sample with a fully reconstructed single e^+e^- pair is 10 times smaller than the total data sample with at least one pair passing all the data quality cuts and with a 2MIPs cut (see Sec. IVA) in S11.

Similar calculations may be done for the Stokes parameter η_1. If we make a weighted average for the asymmetry values between 20 and 100 GeV, where we expect no asymmetry, we obtain a value of $0.19 \pm 0.3\%$. Above 100 GeV we expect a small asymmetry, where we measured $(1.4 \pm 0.7)\%$ between 100 and 180 GeV.

Using Eq. (16), one can now find the measured circular polarization degree which is equal $\eta_2 = 21 \pm 11\%$. This is consistent with the predicted value of 16%.

The statistical significance of the result was estimated using the F-test to evaluate the confidence level associated with distinguishing between two different statistical distributions. The first distribution was formed by the variance of the energy dependent data for the experimental circular polarization with respect to the theoretical prediction displayed in Fig. 20. The second distribution was formed by the variance of the same data to the null hypothesis prediction of no circular polarization. Limiting the test to the region where the crystal polarimeter has analyzing power, and also to the region where the circular polarimetry technique of Eq. (16) has efficiency (80–110 GeV), then we find a confidence limit of 73% for the observation of circular polarization.

C. Polarization measurement of SOS radiation

This third section of the experiment can be divided in two parts: (1) production of the photon beam by the photon radiation from the 178 GeV electron beam in the Si radiator oriented in the SOS mode and (2) measurement of the linear polarization using diamond crystals as analyzers. Prior to the experiment, Monte Carlo simulations were used to estimate the photon yield, the radiated energy, and the linear polarization of the photon beam and we optimized the orientation of the crystal radiator. The Monte Carlo calculations also included the crystal analyzer to estimate the asymmetry of the e^+e^- pair production. The simulations further included the angular divergence of the electron beam, the spread of 1% in the beam energy, and the generation of the electromagnetic shower that develops in oriented crystals. To optimize the processing time of the Monte Carlo simulation, energy cuts of 5 GeV for electrons and of 500 MeV for photons were applied.

1. Photon beam

The SOS photons were produced as discussed in Sec. II B, and Fig. 3 displays a theoretical calculations of the various components of the photon power yield per unit of thickness of radiator crystal as used in the experiment. However, there are several consequences for the photon spectrum due to the use of a 1.5 cm thick crystal. For the chosen orientation of the relatively thick Si crystal, the emission of mainly low energy photons from planar coherent bremsstrahlung results in a total average photon multiplicity above 15. The most probable radiative energy loss of the 178 GeV electrons is expected to be 80%. The beam energy decreases significantly as the electrons traverse the crystal. The peak energy of both SOS and PC radiation also decreases with the decrease in electron energy. Consequently, the SOS radiation spectrum is not peaked at the energy for a thin radiator, but becomes a smooth energy distribution.

Clearly, many electrons may pass through the crystal without emitting SOS radiation and still lose a large fraction of their energy due to PC and ICB. Hard photons emitted in the first part of the crystal that convert in the later part do not contribute anymore to the high-energy part of the photon spectrum. A full Monte Carlo calculation is necessary to propagate the predicted photon yield with a thin crystal, as shown in Fig. 3 for 178 GeV electrons, to the current case with a 1.5 cm thick crystal. This has been implemented for the measured photon spectrum shown in Fig. 23. We see that the measured SOS photon spectrum shows a smoothly decreasing distribution. Consequently, the high-energy radiation is emitted essentially in the very first part of the crystal, while soft photons will be emitted along the full length of the crystal. This effect has been observed previously [16]. The low energy region of the photon spectrum is especially saturated, due to the abun-

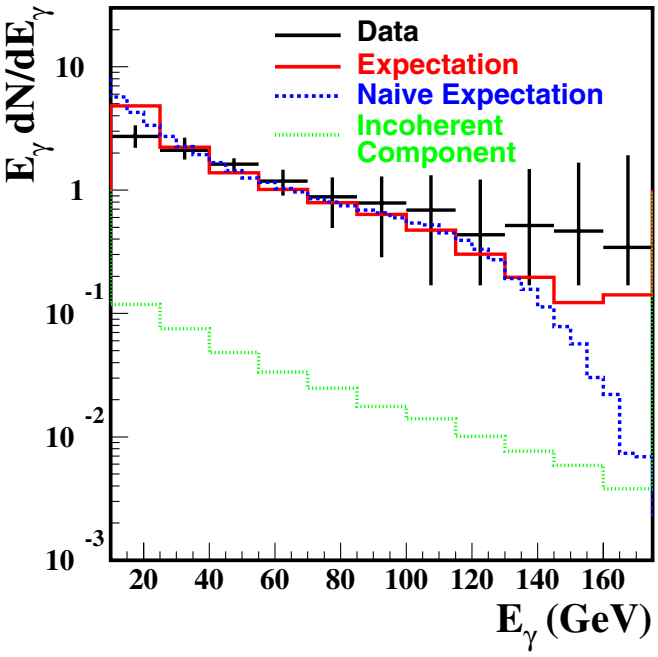

FIG. 23. (Color) Photon power yield, $E_\gamma dN/dE_\gamma$, as a function of the energy E_γ of individual photons radiated by an electron beam of 178 GeV in the SOS-aligned 1.5 cm Si crystal. The black crosses are the measurements with the pair spectrometer, the vertical lines represent the errors including the uncertainty in the acceptance of the spectrometer. The red solid histogram represents the Monte Carlo prediction for our experimental conditions. The green dotted line represents the small contribution due to incoherent interactions. For completeness, we also show the theoretical predictions if the experimental effects are ignored (blue dashed line).

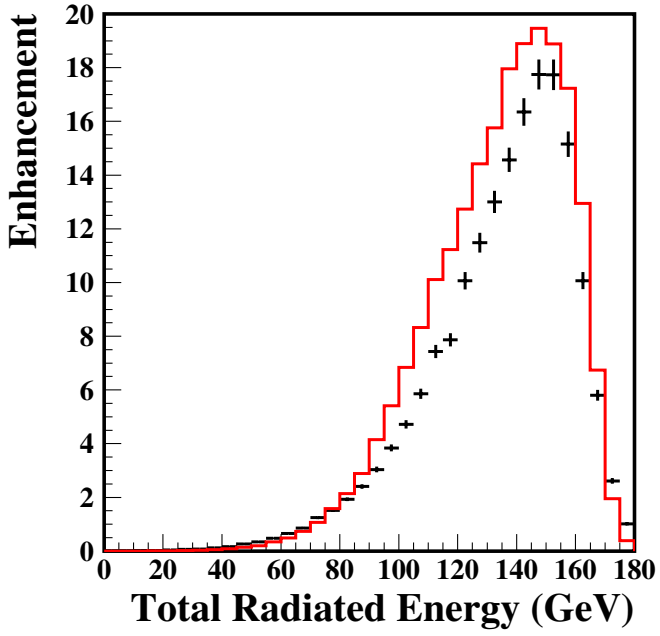

FIG. 24. (Color) Enhancement of the intensity with respect to the Bethe-Heitler (ICB) prediction for randomly oriented polycrystalline Si as a function of the total radiated energy E_{tot} in the SOS-aligned Si crystal by 178 GeV electrons. The black crosses are the measurements and the red histogram represents the Monte Carlo prediction.

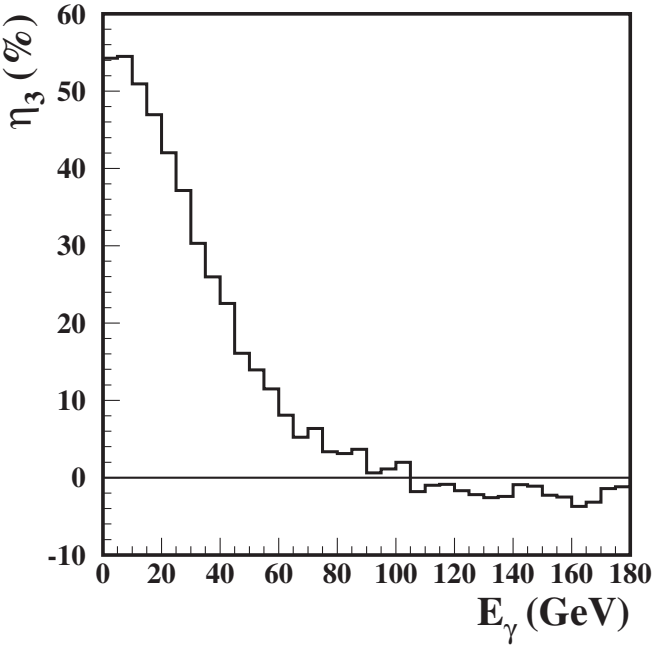

FIG. 25. Expected linear polarization as a function of the energy E_γ of the photons produced in the SOS-aligned Si crystal by 178 GeV electrons.

dant production of low energy photons. Above 25 GeV however, there is satisfactory agreement with the theoretical Monte Carlo prediction, which includes the effects mentioned above.

The enhancement of the emission probability compared to the ICB prediction is given in Fig. 24 as a function of the total radiated energy as measured in the calorimeter. The maximal enhancement is about a factor of 18 at 150 GeV and corresponds well with the predicted maximum of about 20 at 148 GeV. This is a multiphoton spectrum measured with the photon calorimeter. The peak of radiated energy is situated at 150 GeV, which means that each electron lost about 80% of its initial energy due to the large thickness of the radiator. This means that the effective radiation length of the oriented single crystal is several times shorter in comparison with the amorphous target. The low energy region is depleted due to the pileup of several photons.

The radiator angular settings were chosen to have the total linear polarization from the SOS radiation purely along η_3, that is $\eta_1 = 0$. The η_2 component is also zero because the electron beam is unpolarized. The expected η_3 (linear polarization) component of the polarization shown is in Fig. 25 as a function of photon energy. It is well known that channeling radiation in single crystals is linearly polarized [67,68] and the low energy photons up to 70 GeV are also predicted to be linearly polarized in the Monte Carlo simulations. High-energy photons are predicted to have a small degree of polarization.

2. Asymmetry measurement

The polarization measurement was made as explained in Sec. III A. A multitile synthetic diamond crystal was used as an analyzer oriented with the photon beam at 6.2 mrad to the ⟨100⟩ axis and at 465 μrad from the (110) plane. This configuration is predicted to have a maximal analyzing power for a photon energy of 125 GeV as is shown in Fig. 26. The predicted analyzing power in the high-energy peak region is about 30%.

The measured asymmetry and the predicted asymmetry are shown in Fig. 27. One can see that the measured asymmetry is consistent with zero over the whole photon energy range. For the photon energy range of 100–155 GeV, we find less than 5% asymmetry at 90% confidence level using the F-test of significance. The null result is expected to be reliable as the correct operation of the polarimeter has been confirmed in the same beam time in measurements of the polarization of CB radiation as described in Sec. V A. Note that the expected asymmetry is small, especially in the high-energy range of 120–140 GeV, where the analyzing power is large, see Fig. 26. This corresponds to the expected small linear polarization in the high-energy range, see Fig. 25.

In contrast to the result of a previous experiment [36], our results are consistent with calculations that predict a polarization of only a few percent in the high-energy photon peak for the SOS orientation. The analyzing power of the diamond analyzer crystal in the previous experiment's [36] setup peaked in the photon energy range of 20–40 GeV where a high degree of linear polarization is

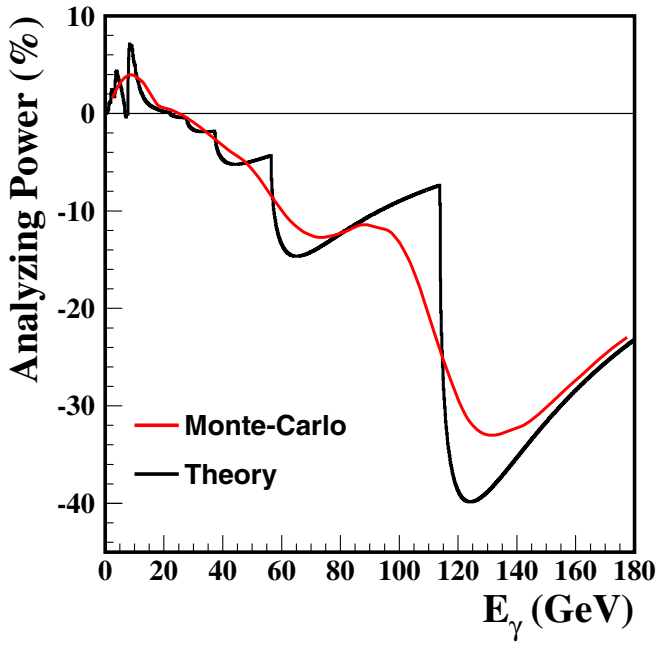

FIG. 26. (Color) Analyzing power R with the aligned diamond crystal as a function of the photon energy E_γ (black curve) for an ideal photon beam without angular divergence and (red curve) for the Monte Carlo simulation of photons with the beam conditions in the actual experiment.

expected. However, for that experiment in the high-energy photon region we expect a small analyzing power of about 2%–3%, also following recent calculation [38,56]. The constant asymmetry measured in a previous experiment [36] over the whole range of total radiated energy may therefore not be due to the contribution of the high-energy photons.

From Fig. 25, one can expect a large linear polarization for photons in the low energy range of 20–50 GeV.

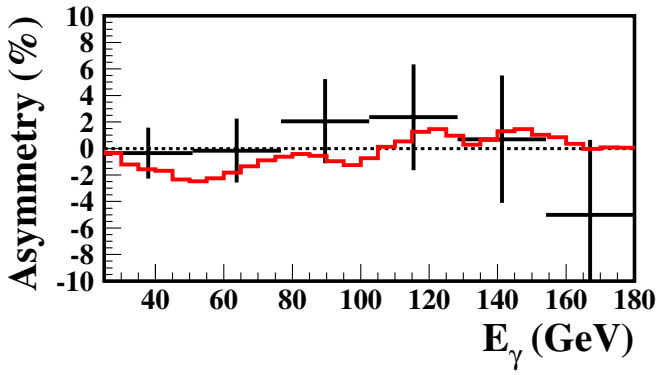

FIG. 27. (Color) Asymmetry of the e^+e^- pair production in the aligned diamond crystal as a function of the photon energy E_γ which is measured to determine the P_1 component of the photon polarization in the SOS-aligned Si crystal by 178 GeV electrons. The black crosses are the measurements and the red histogram represents the Monte Carlo prediction.

However, the analyzing power was optimized for an photon energy of 125 GeV and is small in the region where we expect a large polarization. A different choice of orientation of the analyzer crystal can move the analyzing power peak to the low energy range and may be used to measure the linear polarization in the low energy range.

VI. CONCLUSIONS

A. Birefringence in CPP and a new crystal polarimetry

Our results presented in the previous section show the feasibility of aligned crystals for linearly polarized high-energy photon beams. From the experimental point of view, for the creation of a photon beam with a predictable spectrum the crucial components are (i) high precision goniometers to align the radiator crystal with respect to the electron beam and (ii) tracking chambers to monitor the incident angles of the electron beam on the crystal surface. The predictability of the photon energy and polarization is a good asset for designing future beam lines and experiments. The results also establish the applicability of aligned crystals as polarimeters for an accurate measurement of the photon polarization at high energies. The important aspects are the selection of the analyzer material and the utilization of quasisymmetric pairs. The use of available synthetic diamond as analyzer crystal is found to be very promising due to its durability and high analyzing power.

The pair spectrometer enables us to do asymmetry measurements for single photons in a multiphoton environment. If the photon multiplicity is low, as it would be for laser generated beams with $E > 10$ GeV, then a simple multiplicity detector can be used to replace the more complex pair spectrometer. This is especially the case for a multiplicity detector which is energy selective. CB events with high photon multiplicity are known to be dominated by a single high-energy photon and accompanied by multiple low energy photons.

The crystal polarimetry technique developed here will also be applicable in high-energy photon beam lines as a fast monitoring tool. For example, in a future $\gamma\gamma$ or $e\gamma$ collider quasi-online monitoring of the photon beam polarization could be achieved using this crystal polarimetry method. In the most competitive designs of such colliders [69], the photon beam after the interaction region is transferred to a beam dump; hence, the destructive nature of the crystal polarimetry technique does not constitute an impediment for its utilization.

B. Conversion of linear to circular polarization

The experimental results of this section show that coherence effects in single crystals can be used to transform linear polarization of high-energy photons into circular polarization and vice versa. Thus, it seems possible to produce circularly polarized photon beams with energies

above 100 GeV at secondary (unpolarized) electron beams at high-energy proton accelerators. The birefringent effects become more pronounced at higher photon energy, which allows for thinner crystals with higher transmittance.

Diamond will be more efficient than silicon as quarter wave plates, and a 2 cm thick diamond crystal will have a transmission probability of about 80% for 100 GeV photons. A diamond array of 0.4 cm thickness was produced and aligned for our experiments, where we used it as a linear polarization analyzer, see Fig. 6.

A robust measurement of the circular polarization would involve measurement of the decay asymmetry of ρ-mesons produced in and behind the birefringent Si crystal. An alternative method was used here. The aligned pair-production crystal was used as an analyzer, and realistic theoretical calculations describe very well (i) the radiated photon spectrum from the aligned radiator and (ii) the pair-production asymmetries in the aligned analyzer with and without the birefringent Si crystal in the photon beam. In view of this good agreement all the predicted effects, including the birefringent effect, seem to be confirmed by the present measurements. Measurements of the charged particle multiplicity with depleted Si detectors show a large sensitivity to crystal alignments and can be used to control the alignment of crystals and the photon polarization in a future polarimeter setup.

C. Polarization measurement of SOS radiation

We have performed an investigation of both enhancement and polarization of photons emitted in the so-called SOS radiation mode. This is a special case of coherent bremsstrahlung for multihundred GeV electrons incident on oriented crystalline targets, where the hardness and the enhancement of the photon spectrum is more favorable than in the normal CB case. The experimental setup had the capacity to deal with the relatively high photon multiplicity and single photon spectra were measured. This is very important in view of the fact that there are several production mechanisms for multiple photons which have different radiation characteristics. We have confirmed the single photon nature of the hard photon peak produced in SOS radiation.

The issue of the polarization of the SOS photons had previously not been settled conclusively. The results of an earlier experiment [36] indicated that a large polarization might be obtained for the high-energy SOS photons. Our experimental results show that the high-energy photons emitted by electrons passing through the Si crystal radiator oriented in the SOS mode have a linear polarization smaller than 20% at a confidence level of 90%.

Since the previous experiments, the theoretical situation for the polarization of hard SOS photons has also become clearer. Our results also confirm these recent calculations which predict that the linear polarization of high-energy photons created in SOS orientation of the crystal is small compared to the polarization obtained with the PE orientation.

Photon emission by electrons traversing single crystals oriented in the SOS orientation has interesting peculiarities since three different radiation processes are involved: (1) incoherent bremsstrahlung, (2) channeling radiation, and (3) coherent bremsstrahlung induced by the periodic structure of the atomic strings in the crystal that are crossed by the electron. The recent calculations have taken these three processes into account and predict around a 5% polarization for the high-energy SOS photons. This prediction is consistent with our zero polarization result from the asymmetry measurement of single photons with energies above 100 GeV.

ACKNOWLEDGMENTS

We express our gratitude to CNRS, Grenoble, for the crystal alignment and Messers DeBeers Corporation for providing the high quality synthetic diamonds. We are grateful for the help and support of N. Doble, K. Elsener, and H. Wahl. It is a pleasure to thank the technical staff of the participating laboratories and universities for their efforts in the construction and operation of the experiment. This research was partially supported by the Illinois Consortium for Accelerator Research, Agreement No. 228-1001. U. I. U. acknowledges support from the Danish Natural Science research council. The support of the National Research Foundation of South Africa is also acknowledged.

[1] G. Baum *et al.*, Compass Proposal, CERN/SPSLC 96-14, SPSLC/P297, 1996.
[2] Proposal on Spin Physics Using the RHIC Polarized Collider (RHIC-Spin Collaboration) (1992), update 1993.
[3] V. Ghazikhanian *et al.*, SLAC Proposal E-159/160/161, 2000.
[4] A. Afanasev, C. E. Carlson, and C. Wahlquist, Phys. Rev. D **58**, 054007 (1998).
[5] H. Olsen and L. C. Maximon, Phys. Rev. **114**, 887 (1959).
[6] I. M. Nadzhafov, Bull. Acad. Sci. USSR, Phys. Ser. **14**, 2248 (1976).
[7] A. B. Apyan, R. Avakian, P. Bosted, S. Darbinian, and K. Ispirian, Nucl. Instrum. Methods Phys. Res., Sect. B **145**, 142 (1998).
[8] U. I. Uggerhøj, Rev. Mod. Phys. **77**, 1131 (2005).
[9] R. Alley *et al.*, Nucl. Instrum. Methods Phys. Res., Sect. A **365**, 1 (1995).
[10] J. L. Turner *et al.*, SLAC-PUB-9235, 2002.
[11] J. Lindhard, K. Dan. Vidensk. Selsk. Mat. Fys. Medd. **34**, 1 (1965).
[12] V. N. Baier, V. M. Katkov, and V. M. Strakhovenko, *Electromagnetic Processes at High Energies in Oriented Single Crystals* (World Scientific, Singapore, 1998).
[13] A. Apyan *et al.*, arXiv:hep-ex/0306028.
[14] A. Apyan *et al.*, arXiv:hep-ex/0306041.

[15] A. Apyan *et al.*, arXiv:hep-ex/0406026.
[16] K. Kirsebom, U. Mikkelsen, E. Uggerhøj, K. Elsener, S. Ballestrero, P. Sona, S. H. Connell, J. P. F. Sellschop, and Z. Z. Vilakazi, Nucl. Instrum. Methods Phys. Res., Sect. B **174**, 274 (2001).
[17] B. Ferretti, Nuovo Cimento **7**, 118 (1950).
[18] M. L. Ter-Mikaelian, *High Energy Electromagnetic Processes in Condensed Media* (Wiley Interscience, New-York, 1972).
[19] H. Uberall, Phys. Rev. **103**, 1055 (1956).
[20] G. Diambrini-Palazzi, Rev. Mod. Phys. **40**, 611 (1968).
[21] L. Criegee, G. Lutz, H. D. Schulz, U. Timm, and W. Zimmermann, Phys. Rev. Lett. **16**, 1031 (1966).
[22] P. Bussey, C. Paterson, C. Raine, R. Hughesjones, G. Lafferty, J. Lane, and D. Mercer, Nucl. Instrum. Methods Phys. Res. **211**, 301 (1983).
[23] H. Bilokon, G. Bologna, F. Celani, B. P. R. Falcioni, G. Mannocchi, and P. Picchi, Nucl. Instrum. Methods Phys. Res. **204**, 299 (1983).
[24] A. Apyan, Nucl. Instrum. Methods Phys. Res., Sect. B **255**, 269 (2007).
[25] R. Morin, *Monte Carlo Simulation in the Radiological Sciences* (CRC Press, Boca Raton, Florida, 1988).
[26] R. Medenwaldt *et al.*, Phys. Lett. B **281**, 153 (1992).
[27] J. Schwinger, Phys. Rev. **75**, 1912 (1949).
[28] J. Schwinger, Proc. Natl. Acad. Sci. U.S.A. **40**, 132 (1954).
[29] J. Schwinger, Phys. Rev. D **7**, 1696 (1973).
[30] A. Sorensen, Nucl. Instrum. Methods Phys. Res., Sect. B **119**, 1 (1996).
[31] Y. V. Kononets, Nucl. Instrum. Methods Phys. Res., Sect. B **33**, 22 (1988).
[32] K. Kirsebom, U. Mikkelsen, E. Uggerhøj, K. Elsener, S. Ballestrero, P. Sona, and Z. Vilakazi, Phys. Rev. Lett. **87**, 054801 (2001).
[33] A. Baurichter *et al.*, Phys. Rev. Lett. **79**, 3415 (1997).
[34] K. Kirsebom *et al.*, Nucl. Instrum. Methods Phys. Res., Sect. B **119**, 79 (1996).
[35] A. Saenz and H. Uberall, *Coherent Radiation Sources* (Springer-Verlag, Berlin, 1985).
[36] K. Kirsebom *et al.*, Phys. Lett. B **459**, 347 (1999).
[37] V. N. Baier, V. M. Katkov, and V. M. Strakhovenko, Nucl. Instrum. Methods Phys. Res., Sect. B **69**, 258 (1992).
[38] S. M. Darbinian and N. L. Ter-Isaakian, Nucl. Instrum. Methods Phys. Res., Sect. B **187**, 302 (2002).
[39] V. M. Strakhovenko, arXiv:hep-ph/0301149.
[40] V. M. Strakhovenko, Phys. Rev. A **68**, 042901 (2003).
[41] A. Apyan (private communication).
[42] G. Barbiellini, G. Bologna, G. Diambrini, and G. Murtas, Nuovo Cimento **28**, 435 (1963).
[43] R. Moore *et al.*, Nucl. Instrum. Methods Phys. Res., Sect. B **119**, 149 (1996).
[44] A. B. Apyan, R. Avakian, S. Darbinian, K. Ispirian, S. Taroian, U. Mikkelsen, and E. Uggerhøj, Nucl. Instrum. Methods Phys. Res., Sect. B **173**, 149 (2001).
[45] K. Kirsebom *et al.*, Nucl. Instrum. Methods Phys. Res., Sect. B **135**, 143 (1998).
[46] R. Burns, V. Cvetkovic, C. Dodge, D. Evans, M. Rooney, P. Spear, and C. Welbourn, J. Cryst. Growth **104**, 257 (1990).
[47] J. P. F. Sellschop *et al.*, New Diamond and Frontier Carbon Technology **10**, 253 (2000).
[48] J. P. F. Sellschop, A. Freund, J. Hoszowska, S. H. Connell, M. Rebak, and R. C. Burns, Phys. Status Solidi A **193**, 415 (2002).
[49] A. Apyan *et al.*, Reports No. CERN/SPSC 98-17 and No. SPSC/P308, 1998.
[50] G. Unel *et al.*, Int. J. Mod. Phys. A **16**, 1071 (2001), Suppl. 1C.
[51] N. Cabibbo, G. D. Prato, G. D. Franceschi, and U. Mosco, Phys. Rev. Lett. **9**, 270 (1962).
[52] G. D. Zorzi, G. Diambrini-Palazzi, and A. D. Domenico, Polarization at LEP, CERN **2**, 64 (1988).
[53] Y. V. Kononets (private communication).
[54] V. A. Maisheev, arXiv:hep-ex/9904029.
[55] N. Z. Akopov, A. B. Apyan, and S. Darbinyan, arXiv:hep-ex/0002041.
[56] V. M. Strakhovenko, Nucl. Instrum. Methods Phys. Res., Sect. B **173**, 37 (2001).
[57] J. Spanggaard, CERN Report No. SL-Note-98-023, 1998.
[58] R. Groess, Master's thesis, University of Witwatersrand, South Africa, 2001.
[59] O. Wessley, Master's thesis, University of Witwatersrand, South Africa, 2001.
[60] I. B. G.Ünel, I. Birol, and S. Ballestrero, IEEE Trans. Nucl. Sci. **51/4**, 1482 (2004).
[61] I. B. G. Ünel, I. Birol, and S. Eichblatt, IEEE Trans. Nucl. Sci. **51/4**, 1449 (2004).
[62] W. Heitler, *The Quantum Theory of Radiation* (Dover Publications, New York, 1984).
[63] N. Cabibbo, G. D. Prato, G. D. Franceschi, and U. Mosco, Nuovo Cimento **27**, 979 (1963).
[64] C. Berger *et al.*, Phys. Rev. Lett. **25**, 1366 (1970).
[65] R. Eisele, D. Sherden, R. Siemann, C. Sinclair, D. Quinn, J. Rutherfoord, and M. Shupe, Nucl. Instrum. Methods Phys. Res. **113**, 489 (1973).
[66] A. Apyan *et al.*, Nucl. Instrum. Methods Phys. Res., Sect. B **234**, 128 (2005).
[67] Y. N. Adishchev, I. Vnukov, S. Vorobev, V. Golovkov, V. Zabaev, V. Lunev, and A. Kurkov, JETP Lett. **33**, 462 (1981).
[68] S. A. Vorobyov *et al.*, Sov. Phys. JETP **94**, 38 (1988).
[69] NLC Zeroth Design Report, SLAC Report No. 474 (1996); Tesla Conceptual Design Report, DESY 1997-048, 1997.